Fundamentals of reservoir surface energy as related to surface properties, wettability, capillary action, and oil recovery from fractured reservoirs by spontaneous imbibition

DE-FC26-03NT15408

Semi-Annual Report
07/01/2007 – 12/31/2007

Norman R. Morrow, Principal Investigator
Yu Li
Geoffrey Mason
Douglas Ruth
Evren Unsal
Siluni Wickramathilaka
Shaochang Wo
Peigui Yin

January 2008

Submitted by:
Chemical & Petroleum Engineering
University of Wyoming
Dept. 3295, 1000 E. University Ave
Laramie, WY 82071

Disclaimer

ABSTRACT

The objective of this project is to increase oil recovery from fractured reservoirs through improved fundamental understanding of the process of spontaneous imbibition by which oil is displaced from the rock matrix into the fractures. Spontaneous imbibition is fundamentally dependent on the reservoir surface free energy but this has never been investigated for rocks. In this project, the surface free energy of rocks will be determined by using liquids that can be solidified within the rock pore space at selected saturations. Thin sections of the rock then provide a two-dimensional view of the rock minerals and the occupant phases. Saturations and oil/rock, water/rock, and oil/water surface areas will be determined by advanced petrographic analysis and the surface free energy which drives spontaneous imbibition will be determined as a function of increase in wetting phase saturation. The inherent loss in surface free energy resulting from capillary instabilities at the microscopic (pore level) scale will be distinguished from the decrease in surface free energy that drives spontaneous imbibition.

A mathematical network/numerical model will be developed and tested against experimental results of recovery versus time over broad variation of key factors such as rock properties, fluid phase viscosities, sample size, shape and boundary conditions. Two fundamentally important, but not previously considered, parameters of spontaneous imbibition, the capillary pressure acting to oppose production of oil at the outflow face and the pressure in the non-wetting phase at the no-flow boundary versus time, will also be measured and modeled. Simulation and network models will also be tested against special case solutions provided by analytic models.

In the second stage of the project, application of the fundamental concepts developed in the first stage of the project will be demonstrated. The fundamental ideas, measurements, and analytic/numerical modeling will be applied to mixed-wet rocks. Imbibition measurements will include novel sensitive pressure measurements designed to elucidate the basic mechanisms that determine induction time and drive the very slow rate of spontaneous imbibition commonly observed for mixed-wet rocks. In further demonstration of concepts, three approaches to improved oil recovery from fractured reservoirs will be tested; use of surfactants to promote imbibition in oil wet rocks by wettability alteration: manipulation of injection brine composition: reduction of the capillary back pressure which opposes production of oil at the fracture face.

TABLE OF CONTENTS

INTRODUCTION

Objectives

The long-range objective of this project is to improve oil recovery from fractured reservoirs through improved fundamental understanding of the process of spontaneous imbibition by which oil is displaced from the rock matrix into the fractures. Spontaneous imbibition is fundamentally dependent on the surface energy. An initial objective is to determine the surface energy and relate the dissipation of surface energy to the mechanism of spontaneous imbibition. A parallel objective is to model the mechanism of spontaneous imbibition by a combination of network analysis and numerical modeling. Also fundamentally important, but not previously considered, parameters of spontaneous imbibition, the capillary pressure acting to oppose production of oil at the outflow face and the pressure in the non-wetting phase at the no-flow boundary (in effect within oil in the non-invaded zone of the rock matrix) versus time, will also be measured and compared with values predicted by the mathematical model. The next objective is to measure surface energy and related spontaneous imbibition phenomena for mixed-wettability rocks prepared by adsorption from crude oil. The dissipation of surface free energy must then be related to oil production at mixed-wet conditions. The final objective is to apply the results of the project to improved oil recovery from fractured reservoirs in three ways: reduction of the capillary force that opposes oil production at the fracture face; change in wettability towards increased water wetness; identification of conditions where choice of invading brine composition can give improved recovery.

TASKS

Budget period 1, July 1, 2003 through June 30, 2005 – Ideas and Concept development: Fundamentals of Spontaneous Imbibition

Task 1. *Work of displacement and surface free energy.* Obtain complementary sets of capillary pressure drainage and imbibition data and data on changes in rock/brine, rock/oil, and oil/brine interfacial areas with change in saturation for drainage and imbibition for at least two rock types (sandstone and carbonate). Determine free-energy/work-of-displacement efficiency parameters for drainage and imbibition for at least two rock types so that changes in rock/wetting phase/non-wetting phase surface areas can be closely estimated from capillary pressure measurements.

Task 2. *Imbibition in simple laboratory and mathematical network models.* Study imbibition in at least three simple tube networks that can be modeled analytically to establish and/or confirm fundamental aspects of the pore scale mechanism of dynamic spontaneous imbibition with special emphasis on determining how spontaneous imbibition is initiated and the key factors in how the saturation profile develops with time. Incorporate rules developed from laboratory measurements on relatively simple networks into the design of a computational network model. Use the network model to obtain an account of the mechanism by which imbibition is initiated, the saturation profile is developed, and the rate of spontaneous imbibition in terms of the dissipation of surface free energy that accompanies change in saturation.

Task 3. *Novel observations on fluid pressures during imbibition and the mechanism of non-wetting phase production at the imbibition face.* Make novel observations on the imbibition mechanism including details of the mechanism of oil production at the outflow rock face and the change in the non-wetting phase pressure at the no-flow boundary of the core during the course of spontaneous imbibition for at least 16 distinct combinations of rock/ fluid properties.

Task 4. *Network/numerical model and new imbibition data.* Develop a numerical simulator specifically designed for spontaneous imbibition. Incorporate the network model to obtain a network/numerical model that includes matching the measured pressure in the non-wetting phase at the no-flow boundary, and the pressure that opposes production of oil at the open rock face. Imbibition data will be obtained for at least 10 rocks with over six-fold variation in permeability, and at least 6 orders of magnitude variation in viscosity ratio, and at least 10 variations in sample size, shape, and boundary conditions.

Task 5. *Comparison with similarity solutions.* Compare results given by simulation with special case analytic results given by similarity solutions for spontaneous imbibition for at least five distinct cases of rock and fluid properties.

Budget Period 2, July 1, 2005 through June 30, 2008 - Demonstration of concept: Application to mixed wettability rocks and improved oil recovery from fractures reservoirs.

Task 6. *Rock preparation and Work of displacement and surface areas*
Obtain a range of rock types and identify and obtain crude oils that induce stable mixed wettability. Prepare at least 25 rocks with mixed wettability through crude oil/brine/rock interactions. Determine work of displacement for drainage and imbibition and measure the variation in rock/brine, rock/oil, and oil/brine interfacial areas during the course of drainage and imbibition for at least two examples of mixed wettability.

Task 7. *Novel imbibition measurements on mixed-wet rock and network models.* Obtain, for at least six mixed-wet rocks, spontaneous imbibition data that includes measurements of the non-wetting phase pressure at the no-flow boundary, observations on the capillary pressure that resists production at the open rock face.

Task 8. *Application of network/numerical model to mixed wet rocks.* Use network models to relate dissipation of surface energy to rate of spontaneous imbibition and to account for the frequently observed induction time prior to the onset of spontaneous imbibition into mixed wettability rocks.

Task 9. *Increased oil recovery by spontaneous imbibition.* The mechanism of increased recovery from mixed wet rocks by use of surfactants that promote spontaneous imbibition by favorable wettability alteration will be investigated for at least four distinct examples of crude oil/brine/rock/surfactant combinations. The mechanism of increased recovery by manipulation of brine composition will be investigated for at least four crude oil/brine/rock combinations. Addition of very low concentration surfactants to the imbibing aqueous phase will be explored as a means of increasing the rate of oil recovery by reducing the capillary forces which resist

production of oil at the fracture face. At least twelve combinations of rock and fluid properties including both very strongly wetted and mixed wet rocks will be tested.

EXECUTIVE SUMMARY

Investigation of the driving force for spontaneous imbibition has moved to determination of capillary driving pressures for strongly water wet and mixed wet conditions. An extended interpretation of the pressures that drive imbibition is presented under Task 6. Under Task 7, a new design of imbibition cells has been built which, from the theory presented under Task 8 will use a sample shape that will minimize the effects of sample hetrogeneity. A new theory is also presented for calculation of characteristic length with special attention to the complex flow behavior in cylindrical cores, these being the most commonly used shape in imbibition tests.

Under Task 9, the first measurements of imbibition driving pressures for an aqueous phase containing a surfactant are presented. This approach provides a powerful method of determining the active driving pressure and the extent to which surfactants at the imbibition front are depleted as imbibition progresses. Although capillary driving forces are reduced because of lowered interfacial tension imbibition rates and extent of recovery were increased.

PROGRESS BY TASK - BUDGET PERIOD 2

Task 6. *Rock preparation and work of displacement and surface areas*

Note: Some of the following information has been submitted in previous reports, but the interpretation has been extended and has been submitted for publication.

Counter-current spontaneous imbibition (COUCSI) in porous media is driven by capillary forces. Capillary action results in a high capillary imbibition pressure at the imbibition front and a low capillary drainage pressure at the outlet face. It is the difference between these two pressures that draws in the wetting phase and pushes out the non-wetting phase. A novel technique of measuring the capillary pressure developed at an imbibition front under restricted flow conditions has been applied to Berea sandstones with a range of permeabilities. In the experiments, brine was the wetting phase and refined oil was the nonwetting phase. One end face of a sandstone core was butted to a short section of a finer-pored rock. The composite core surface was then sealed, apart from the end face of the low permeability segment. A connection to a pressure transducer was set in the opposite end face of the core. In most cases, the finer-pored segment was filled with brine. Initially, the main core segment was filled with oil. Imbibition was started by immersing the core in brine. Non-wetting phase could not escape at the open face when the segment of finer-pored rock restricted its movement. For some tests there was an initial period of co-current spontaneous imbibition (COCSI) created by allowing production of non-wetting phase through an outlet tapping in the sealed end face. The outlet was then connected to the transducer and the imbibition changed to COUSCI. There followed an increase in the monitored end pressure to a maximum as fluid redistributed within the core. For the tests in which the fine-pored segments were pre-saturated with brine, even without an initial period of co-current imbibition, limited invasion of the main core segment by brine resulted in an asymptotic rise of the end pressure to a maximum as the imbibition front dispersed. Distance of advance of the wetting liquid was detected by a series of electrodes. The maximum value of the

end pressure provides an estimate of the capillary pressure at an imbibition front for COUCSI. The maximum capillary pressure generated by the invading fluids ranged from 6.6 *kPa* to 42 *kPa* for sandstone with permeabilities between 1.050 μm^2 and 0.06 μm^2.

Introduction

Imbibition arises in many everyday situations, and can be a dominant mode of production of oil from the rock matrix of fractured reservoirs. In Counter-Current Spontaneous Imbibition (COUCSI), a wetting phase (WP) front spontaneously invades a porous medium and forces the non-wetting phase (NWP) to flow counter to the invading WP. The essence of the process is that a pressure difference, P_c, between the two phases is developed by capillary action and it is at a maximum, P_{cf}, at the displacement front. In the experimental cases when gravity can be ignored, the imbibition capillary pressure is the sole driving force that pulls wetting phase into the porous medium, drives the non-wetting phase out, and also overcomes the opposing drainage capillary pressure at the outlet face. A diagram of the pressure distribution between the open face and the front during unrestricted COUSCI is shown in Figure 6.1.

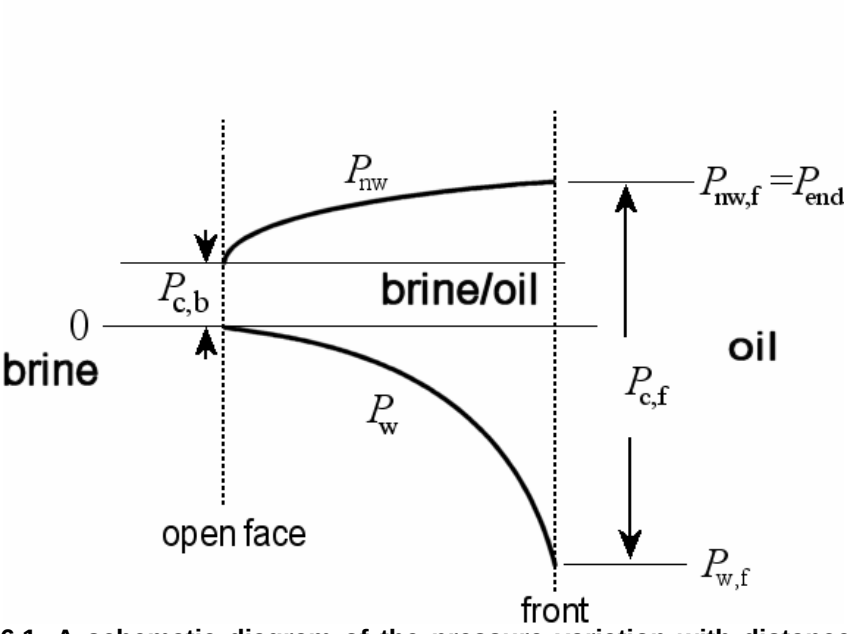

Figure 6.1. A schematic diagram of the pressure variation with distance during counter-current imbibition when the initial water saturation is zero. The pressure drops with distance within the wetting phase. There is a sharp rise in pressure, $P_{c,f}$, when moving from wetting phase to non-wetting phase at the imbibition front. The pressure in the wetting phase declines with distance going back towards the open face. There is a finite pressure, the capillary back pressure, $P_{c,b}$, that is required to produce the droplets of non-wetting phase at the open face.

Imbibition of the WP is in the direction of the positive capillary pressure gradient. The effective frontal capillary pressure is highest at the WP front regardless of the shape of the saturation profile behind it. The lowest capillary pressure is at the open core face; this pressure, where NWP bubbles from the core, is referred to as the capillary back pressure, $P_{c,b}$.

Method

In the absence of gravity and other applied pressures, the capillary pressure at the saturation front ($P_{c,f}$) is the driving force of imbibition. However, this important variable is difficult to measure. The imbibing wetting phase starts to penetrate the bulk of the pore space at the imbibition threshold capillary pressure.

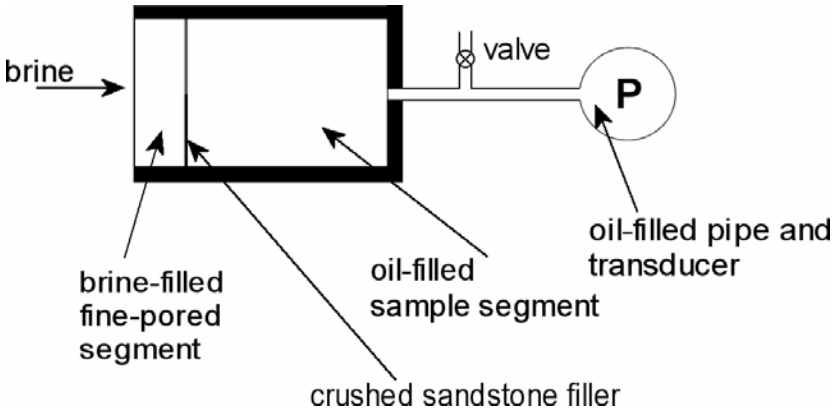

Figure 6.2. Illustration of the measurement technique. A core sample is enclosed by epoxy resin with a butted fine-pored segment of rock at one face. Brine imbibing through the finer-pored segment induces a pressure in the oil which initially fills the main segment. A pressure transducer measures the pressure of the oil in the core.

The technique designed to evaluate $P_{c,f}$ is unusual and is shown schematically in Figure 6.2. Basically a fine-pored rock is butted to the rock under investigation with a means of maintaining hydraulic contact between the segments. The entire surface is sealed, except for one face of the finer-pored segment and a pressure tapping at the opposite end. Imbibition is started in co-current mode by immersing the core, pre-saturated with oil, in brine and disconnecting the tubes to the pressure transducer. COUCSI is started by reconnecting the tubes to the transducer. The end pressure in the oil phase is monitored. The imbibing brine redistributes in the composite core and the pressure rises to a steady value. This is the effective capillary pressure at the imbibition front. Although simple in principle, there are several experimental challenges. The two core segments have to be matched such that the imbibition pressure in the high permeability segment may force oil no more than part way back through the low-permeability segment. However, if the permeability of the segment is too low, then the velocity of the front during any initial period of COSCI will be very slow, prolonging the duration of the experiment. It is important that the position of the front in the high permeability segment be monitored. When the front reaches the pressure tap at the dead end of the core, the measured pressure falls. Ideally, the apparatus should be assembled such that the system contains no gas and that there are no leaks. The pressures are small (10 to 45 *kPa*) and so a sensitive pressure transducer is needed which is capable of working when the pressured side of the membrane is full of liquid.

Consider linear invasion of a wetting phase into a core with only one end face open. By definition, the effective capillary pressure at the WP front, $P_{c,f}$, is the difference in pressure between the non-wetting phase and the wetting phase at the front

$$P_{c,f} = P_{nw,f} - P_{w,f} \quad (6.1)$$

$P_{nw,f}$ is the pressure in the NWP and $P_{w,f}$ is the pressure in the WP, both at the front.
For a core initially saturated with NWP, there is only NWP between the front and the sealed end, P_{end}. Because there is no flow in the dead end pore space, the value of P_{end} is equal to the value of $P_{nw,f}$.

$$P_{end} = P_{nw,f} \quad (6.2)$$

Combining Eq.(2.1) and Eq.(2.2) yields

$$P_{end} = P_{c,f} + P_{w,f} \quad (6.3)$$

When the front is in movement, $P_{w,f}$ must be less than 0 (the pressure value in the WP reservoir) and so

$$P_{end} < P_{c,f} \quad (6.4)$$

If the dispersed front becomes essentially stationary, as will occur with a suitable choice of conditions, the pressure in the WP becomes zero (equal to the pressure value in the WP reservoir) and the pressure in all of the NWP contiguous to the dead end will be constant and equal to P_{end}. So, under the no-flow constraint, the value of the end pressure becomes equal to the value of $P_{c,f}$

$$P_{end} = P_{c,f} \quad (6.5)$$

Ideally, the experiments therefore seek to measure P_{end} when there is no-flow of either WP or NWP in the core.

Experiments

Composite cores

A schematic diagram of the arrangement of the butted core is shown in Figure 6.2. A short segment of low permeability core was chosen which had significantly smaller pores than the main core. It was either a limestone of 0.003 μm^2 permeability with an oil/water breakthrough pressure of 109 *kPa* or a low permeability sandstone of 0.065 μm^2 permeability with a breakthrough pressure of 19 *kPa.* The short segment was butted at the joint with each tested sandstone core, with a 0.1 *cm* thick layer of powder, derived from crushed Berea sandstone, to ensure hydraulic contact. All surfaces of the composite core were sealed with epoxy resin, except for the outer face of the low permeability segment. Except for one case (that presented first in the results), the short segment was initially pre-saturated with WP. This segment served as a semi-permeable membrane that allows WP to enter the core and, ideally, prevents NWP

from leaving at the open face. A nylon tube with an inner diameter of 1.5 mm and an outer diameter of 3 mm, embedded in the otherwise sealed end of the main core, served as a pressure tapping. Details of each composite core are given in Table 6.1. Embedded in the surface of the core and sealed with epoxy resin were a series of electrical tappings. These were used to indicate the advance of the front.

Measurements on composite cores

After assembly, the composite core was immersed in the wetting phase using the arrangement shown in Figure3. The change in pressure in the NWP at the end of the core was monitored with a pressure transducer (Validyne DP15-32 to 40). Saturation changes were determined gravimetrically. The distance of advance of brine into the open core, x_f, was detected from the onset of electrical conductivity between electrodes embedded in the core and an electrode in the brine. All experiments were conducted at room temperature (about 21^oC) and atmospheric pressure (79 kPa).

Some tests were begun with a short period of invasion of wetting phase into the main core segment with the connection fitting on the pressure tap left open to allow flow of oil. After closing this vent, the rise in P_{end} that accompanied transition from COCSI to restricted COUCSI was monitored while the fluids redistributed within the main core segment. The development of the saturation profile for restricted COUCSI was essentially complete, as indicated by a maximum in P_{end}, before the WP reached the far end of the main core.

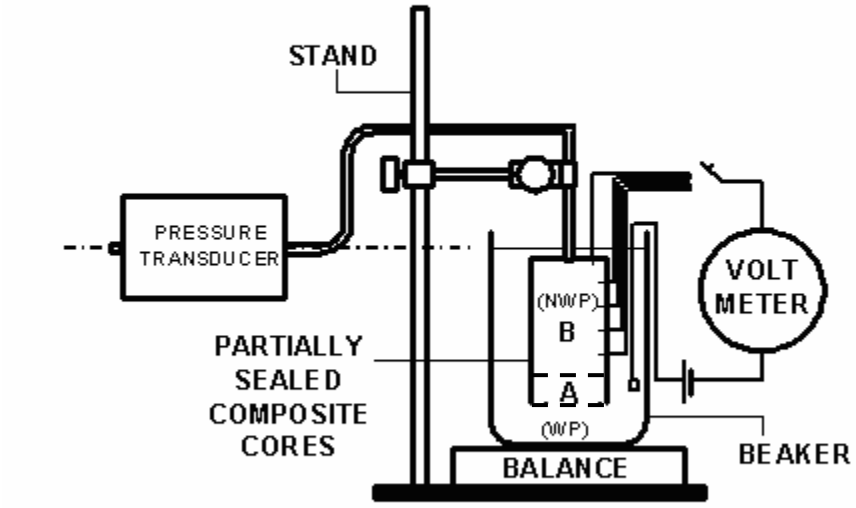

Figure 6.3 Apparatus for measurement of the frontal capillary pressure in COUCSI. A is the low permeability core segment. B is the high permeability core segment. The fitting on the transducer could be loosened to allow oil to escape, thus permitting COCSI. Imbibition of brine into the core was measured by the change in weight indicated by the balance.

Rock and fluid properties

Five Berea sandstones, of 3.8 cm diameter and about 3cm to 7cm in length, with permeabilities ranging from 0.06 μm^2 to 1.067 μm^2 (see Table 1) were tested. All gas permeabilities in Table 6.1 were measured with air under a mean flowing pressure of 15 *kPa*. In one case permeability to oil was measured before and after spontaneous imbibition using standard techniques. Refined oil (Soltrol 220, viscosity 0.0038 *Pa.s*) served as the oil phase. Brine with a salinity of 10,000 ppm NaCl and a viscosity of 0.00115 *Pa.s* was the wetting phase. The interfacial tension between brine and oil was 48.8 *mN/m*.

Table 6.1 Measurement of P_c in COUCSI.

TEST NO.	LOW K CORE ID	D (cm)	L_c (cm)	K (μm^2)	ϕ (%)	MAIN CORE ID	D (cm)	L_c (cm)	K (μm^2)	ϕ (%)	P_{cf} (kPa)	P_{cf}/σ (μm^{-1})
OW1	LS2	3.8	2.07	0.065	17.1	H70	3.8	6.90	1.052	22.1	>12.17	>0.249
OW2	LS3	3.8	2.35	0.065	17.1	H6O	3.8	6.97	1.067	22.2	12.4	0.254
OW3	TL9	3.8	1.84	0.002	16.0	HF4	3.4	3.17	0.964	22.3	14.4	0.295
OW4	TL8B	3.8	1.71	0.003	16.8	M10	3.8	6.00	0.492	20.2	30.0	0.614
OW5	TL3	3.8	1.49	0.003	16.8	L60	3.8	6.18	0.060	19.6	42.0	0.860

Results

Test OW1

In this preliminary test, the two core segments were sealed together and both segments of the composite core were completely filled with oil. After immersion in brine a period of COCSI was allowed by loosening the fitting on the tube to the transducer so that oil was released. Response of an electrode at the joint indicated that the COCSI front had crossed the joint between the segments after 0.45 *hour*. After 2.6 *hours* the front had penetrated 2.75 cm into the high *K* core segment. The fitting on the tube of the transducer was then sealed so that COSCI ceased and imbibition changed to COUCSI. At the start of COUCSI, the end pressure rose quickly and reached its highest value of 12.17 *kPa* after 0.37 *days* (see Figure4). Eventually, oil was seen to appear as droplets at the open face of the low permeability segment and the measured end pressure started to fall. Without this production of oil at the open face, the measured pressure would probable have reached a higher value.

Subsequently the fitting on the tube of the transducer was reopened making the end pressure fall to zero. This transition from COUCSI to COCSI resulted in oil recovery increase from 28% to 48 % within 1.2 days (see Figure 6.4**).**

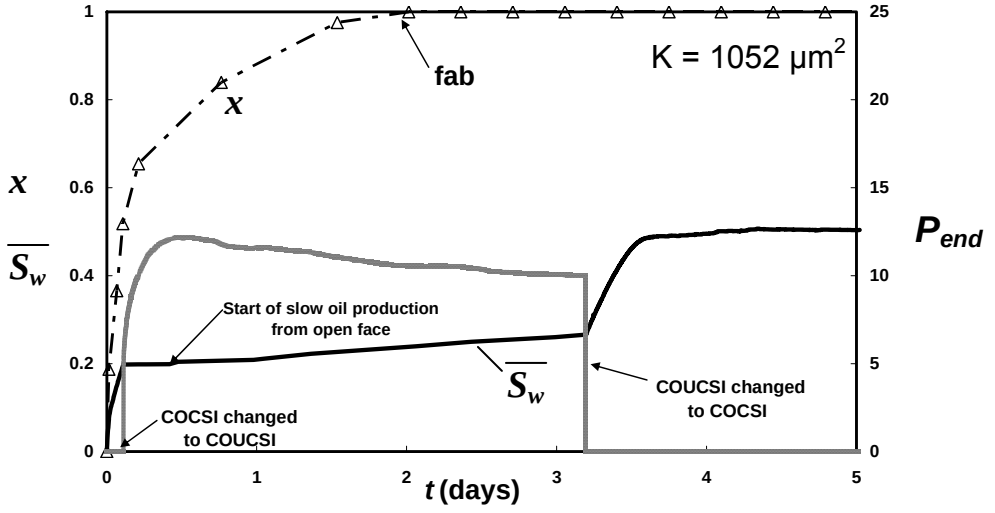

Figure 6.4 Fractional distance of advance of brine, *x*, average brine saturation, $\overline{S_w}$, and end pressure, P_{end}, versus time for Test OW1. The arrival of the front at the end of the core was detected by an electrode and is indicated as "fab" – front at boundary. Imbibition was changed from COUCSI to COCSI after 3.2 days by opening the end tube to atmosphere.

Test OW2

In this test, the cylindrical sides of each segment were separately coated with epoxy. The low-permeability segment was then saturated with brine and the high-permeability segment saturated with oil. The two segments were then epoxied together with a layer of water-saturated crushed sandstone serving to give hydraulic contact between the segments. The main segment in Test OW2 was a duplicate of that used in Test OW1. The composite core was then immersed in brine to initiate the restricted COUCSI imbibition. The end pressure rose to 11 *kPa* within 2 *hrs* and reached its highest value of 12.4 *kPa* after 2.08 *days.* By that time, the front had penetrated 3.25 cm into the high permeability core segment. The pressure was monitored for a further 1.8 days to confirm that the end pressure was stable. There was no production of oil from the open face (unlike Test OW1 in which the low permeability oil segment was initially oil saturated). Nevertheless, the stable end pressure of 12.9 *kPa* was only 0.26 *kPa* higher than the maximum value of P_{end} for Test OW1.

Movement of the water along the core was detected by the onset of electrical conductivity when the brine front contacted a particular electrode. The limited water invasion (see Figure 6.5) by displacement of oil is ascribed mainly to a combination of limited movement of oil into the low permeability segment and compression of gas contained in the tube connected to the pressure transducer. This does not affect the value of the measured pressure. After 3.9 *days*, the core was removed from the apparatus and sawn in half along its axis. An electrode was advanced along the exposed axis of the sliced core. A sudden increase in conductivity showed that the brine had penetrated 3.13 *cm* into the core. It could also be seen that oil had penetrated part way into the low-permeability segment.

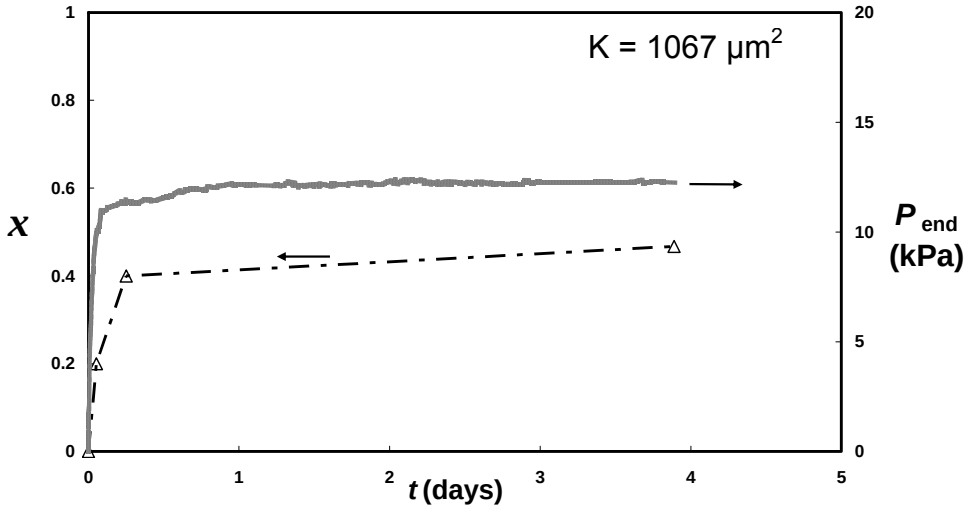

Figure 6.5 Fractional distance of frontal advance along the core, *x*, and end pressure versus time for Test OW2.

Test OW3

The low permeability segment in Test OW3 was set up as in Test OW2 using limestone as the low permeability segment (see Table 1). The main segment was 3.17 *cm* (less than half the main core length used in Test OW2).

Restricted COUCSI imbibition was conducted on the composite core. The end pressure rose to 13.7 *kPa* within 1 *day* and reached its highest value of 14.4 *kPa* after 2 *days* (Figure 6). The front penetrated to the end of the main segment 3.3 *days* after the start of imbibition. The pressure then decreased to 12.55 *kPa* over a further half day.

In Test OW 3, the permeability of the main segment to oil was 0.674 μm^2 when fully saturated with oil. (For Berea sandstone and many other rock types, liquid permeabilities are typically lower than the gas permeability even after correction for slippage.) After imbibition was complete, the core was removed and the low permeability segment and 0.92 cm of the neighboring part of the main core was cut off. The relative permeability to oil of the remaining brine invaded portion of the main core was 0.573 μm^2. Thus, the relative permeability to oil behind the front after imbibition is high, being about 85% of the permeability when fully saturated oil. This implies that the frontal saturation and effective capillary pressure depend on the largest of the invaded pores at the front and their values must be finite during COUCSI. The same conclusion was reached for two-phase flow simulations in 3-D pore-networks (Li et al, 1986).

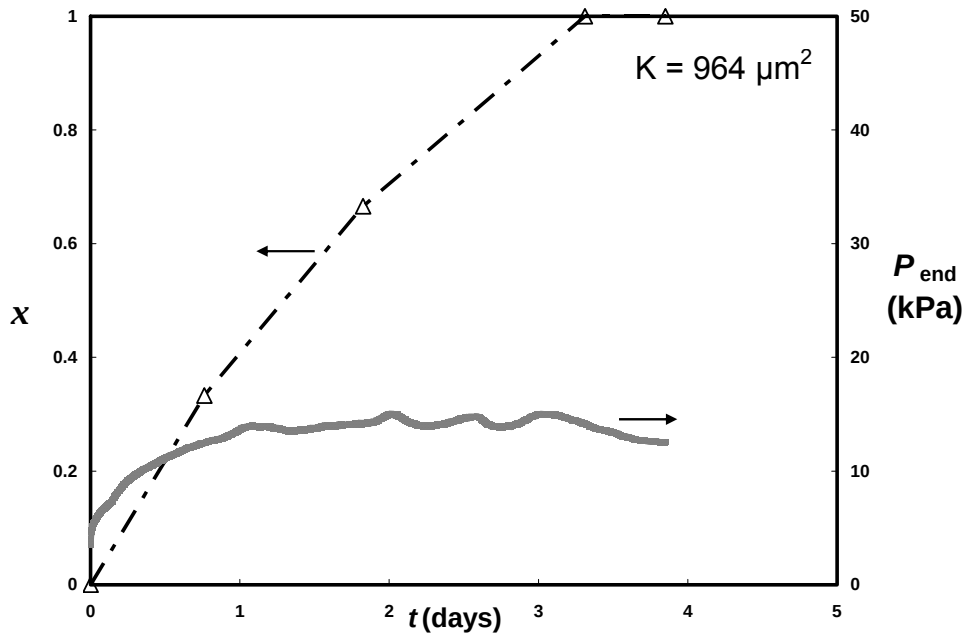

Figure 6.6 Fractional distance of frontal advance along the core, *x*, and end pressure versus time for Test OW3.

Test OW4

The tested sandstone segment was 6 *cm* long with permeability of 0.492 μm^2. A low permeability limestone segment of 1.714 *cm* length and permeability of 0.003 μm^2 was used as the semi-permeable membrane. The low permeability segment was initially saturated with brine as in OW2 and OW3.

The end pressure rose to 29.3 kPa after 1.5 *days* and remained high (see Figure 6.7). After 8 *days*, the electrical conductivity measurement indicated that the brine had penetrated at least 3.6 *cm* into the main segment (x_f/L_c =0.6). The average fractional brine saturation Q_w/V_ϕ of the main segment rose to 0.064. This corresponded approximately to the estimated volumetric compression of a small volume of residual air in the tube connected to the transducer plus the flexure of the transducer diaphragm. As the gas in the tube becomes compressed, the measured end pressure became increasingly sensitive to diurnal variations in ambient pressure and temperature. The overall tendency for decrease in P_{end} after about 7 *days* is ascribed to slight change in core properties with length. After 12 *days*, the fitting near to the transducer was opened and imbibition changed from COUCSI to COCSI; oil recovery increased from 6.4% to 52.4% within 1 *day*.

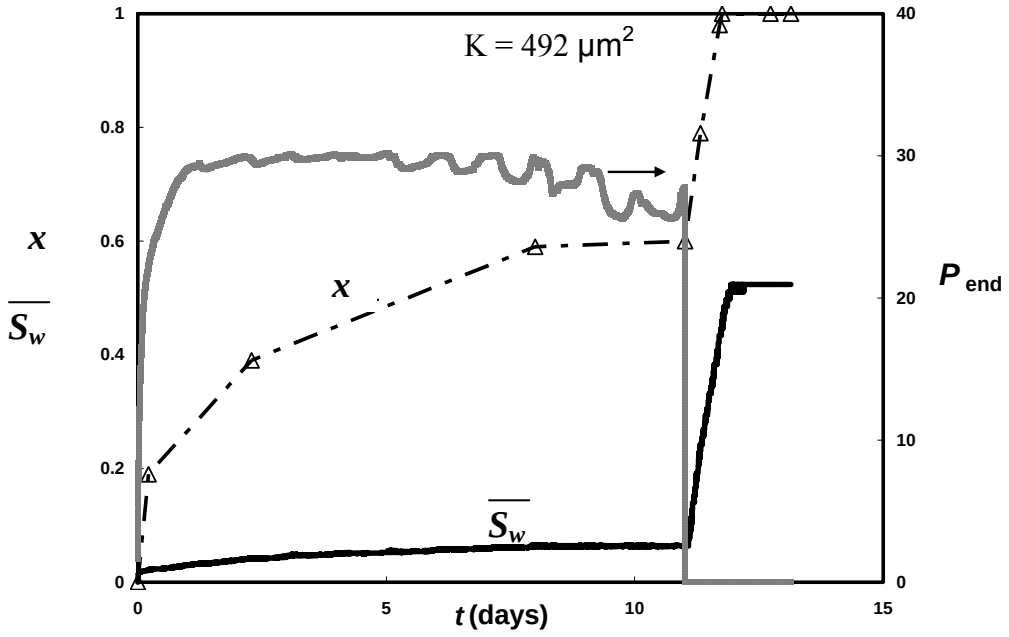

Figure 6.7 Fractional distance of advance of front, *x*, average imbibed brine saturation, $\overline{S_w}$, and end pressure versus time for Test OW4.

Test OW5

The main sandstone segment was 6.175 *cm* long with permeability of 0.06 μm^2. This was the same sandstone that had served as the low permeability segment in Tests OW1 and OW2. A low permeability limestone segment was 1.489 *cm* long and was initially saturated with brine. The end pressure rose very quickly to over 40 *kPa*, within 1.2 *days* and increased only slightly over the next 7 *days* to 42 *kPa* (Figure 6.8). Electrical conductivity indicated that the front had penetrated at least 2.6 *cm* into the main segment 051. ($x_f/L_c = 0.42$). No oil production was observed at the open face throughout the 8 *day* test. Invasion of brine was allowed mainly by compression of some residual gas in the tube to the transducer.

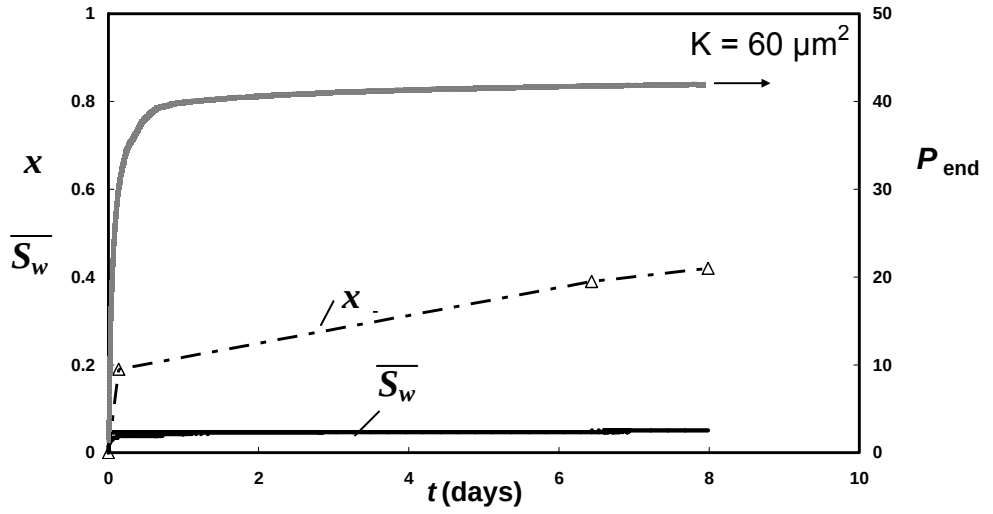

Figure 6.8. Fractional distance of advance of front, *x*, average imbibed brine saturation, $\overline{S_w}$, and end pressure versus time for Test OW5.

Discussion

Dispersion during restricted COUCSI

The transition from COCSI to restricted COUCSI at essentially constant overall saturation is accompanied by dispersion at the front because of capillary action. As the WP advances at the front, the disperse region grows and the NWP pressure increases. WP is drawn into smaller pores previously occupied by NWP and NWP is driven back into the larger pores previously occupied by WP, thus maintaining the mass balance. A remarkable feature of the experimental results is that the end pressure remains essentially constant as the wetting phase redistributes within the core.

Frontal capillary pressures in low permeability Berea sandstone determined by simulation have been reported (Li et al., 2006). The simulation was based on the assumption that the rock pore geometry scaled with grain size making the shapes of the relative permeability and capillary pressure curves similar. The simulations predicted values of P_{cf} that are about half of the maximum pressures measured in the present work.

Dispersion and effective capillary pressure at the imbibition front.

The maximum stable value of P_{end} before the front reaches the end of the core provides an estimate of the effective capillary pressure acting at the imbibition front. The maximum values of P_{end} for Berea sandstones with permeabilities from 1.067 to 0.06 μm^2 ranged from 6.6 to 21.3 *kPa* for water/oil. For strongly wetted systems, the effective pore radius at the front is given by $2\sigma/P_{\text{c,f}}$. An overall pore radius for the core can be obtained from the permeability using the Leverett radius, $2\sqrt{2K/\varphi}$ (Leverett, 1941). If the pore geometry of the sandstones maintains

similarity with change in grain size, a plot of $2\sigma/P_{c,f}$ versus $2\sqrt{2K/\varphi}$ should be a straight line passing through the origin. However, for the four tests OW2 through OW5 for which $P_{c,f}$ was measured, this plot is not linear (Figure 6.8). The inference is that diagenetic changes result in pore sizes and distributions that do not scale linearly with the square root of permeability. Furthermore, the capillary pressure at the front will depend on the largest sections of the smaller pores of the rock, whereas the permeability will depend on the network of the larger pores. Consequently, an exact gradient of unity would not be expected. It is likely that a change in the spread of the pore size distributions of the various sandstones is the main reason for the scatter from linearity in Figure 6.9.

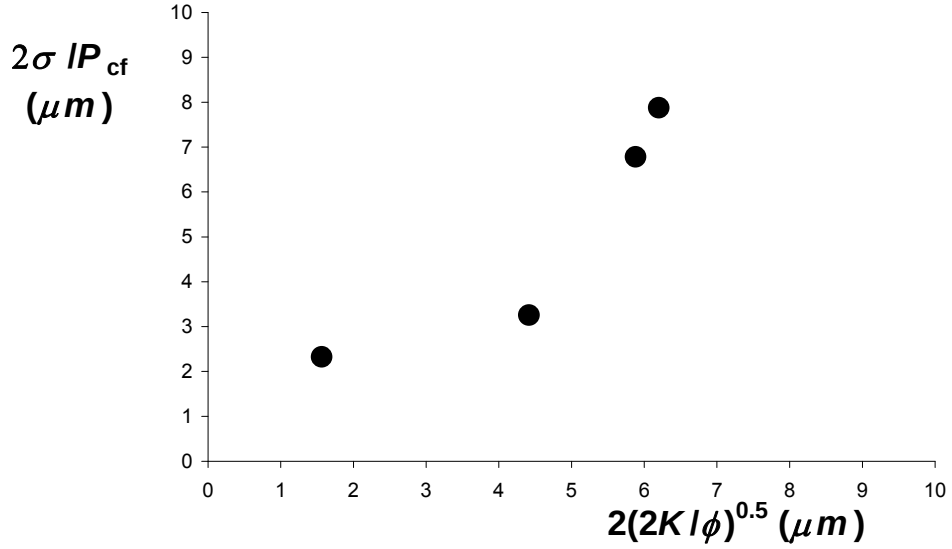

Figure 6.9 The pore radius calculated from the capillary pressure at the front plotted against the pore radius derived from the rock permeability. If the pore geometries of the rocks scaled exactly, this plot would be a straight line. The scatter probably arises from the the effect of diagenetic differences on pore geometry.

Nomenclature

D	core diameter (m)
K	permeability to air (m^2)
L_c	core length (m)
$P_{c,b}$	capillary back pressure (Pa)
$P_{c,f}$	capillary pressure at the imbibition front (Pa)
P_{end}	pressure measured at the dead end (Pa)
$P_{nw,o}$	pressure in non-wetting phase at the open face (Pa)
$P_{nw,f}$	pressure in non-wetting phase at the front (Pa)
Q_w	cumulative input of wetting phase or production of nonwetting phase (m^3)

$\overline{S_w}$ average WP saturation
V_ϕ pore volume (m^3)
x fractional distance along the main core segment
x_f distance along the main core segment (m)

μ_{nw} viscosity of the nonwetting phase ($Pa.s$)
μ_w viscosity of the wetting phase ($Pa.s$)
σ interfacial tension (N/m)
ϕ porosity

Acronyms/abbreviations

WP	wetting phase
NWP	nonwetting phase
COCSI	co-current spontaneous imbibition
COUCSI	counter-current spontaneous imbibition

References

Leverett, M.C.: Capillary behavior in porous solids. Trans Am. Inst. Min. & Met. Eng. 142, 152-169 (1941).

Li, Y., Ruth, D., Mason, G., Morrow, N.R.: Pressures acting in counter-current spontaneous imbibition. J. Pet. Sci. Eng. 52, 87-99 (2006).

Li, Y., Laidlaw, W.C., and Wardlaw, N.C.: Sensitivity of drainage and imbibition to pore structure as revealed by computer simulation of displacement process. Advances in Colloid and Interface Science. 26, 1-68 (1986).

Task 7. *Novel imbibition measurements on mixed-wet rock and network models.*

Discussion

Novel imbibition measurements, some which have been reported previously, have been re-examined in detail particularly with respect to the pressures that control imbibition behavior for both strongly water wet and mixed wet rocks. Analytical studies of counter-current imbibition presented under Task 8 show that the optimum core shape for minimizing the effect of heterogeneities is for a cylinder and with radial imbibition from outside in. An apparatus has been designed and built using this configuration. The test core has a small diameter hole along its axis with facility to measure the end pressure in the nonwetting phase measured by means of a sensitive pressure transducer. Preliminary results are mainly of the expected form.

Task 8. *Application of network/numerical model to mixed wet rocks.*

Results obtained to date for mixed wet rocks (see previous report) demonstrate that although the driving pressure may be very low, imbibition still occurs as a frontal process.

Counter-current imbibition occurs when brine spontaneously displaces oil from a very strongly water-wet rock. Experiments are usually carried out on cylindrical core plugs which have all of their faces open, mainly because this is easiest to do and also because it appears to give the most reproducible results. The flow patterns are complex, but a reasonable approximation can be obtained by assuming piston-like advance of fronts from the radial outer face and both flat ends. This separates the flow pattern into linear imbibition into cones and into radial imbibition into the surrounding toroid ring. Production versus time curves have been calculated for cylinders of varying aspect ratio and other core shapes. The analytical results confirm the experimental observation that sample shape does not have much effect on the shape of the production versus time curves. Bearing in mind the inherent variability of experimental results for individual core samples, the differences would be difficult to detect in experiments. The time for imbibition to be completed scales as the characteristic length. The function given by Ma et al. (1997) requires only a small correction factor for agreement with the analytical result. The present analysis makes straightforward the comparison of results from the complex flow condition of all-faces-open imbibition with results from linear and radial experiments. A comparison is made with published results.

Introduction

Imbibition occurs when the resident fluid in a porous medium (which will be referred to as the non-wetting phase) is spontaneously displaced by a more wetting fluid. When the wetting fluid imbibes into the pores, a saturation front can sometimes be seen. The driving pressure is the capillary pressure produced by interfaces in the pore space. In experiments (Li et al., 2006), a positive pressure can be detected in the non-wetting phase. This pressure pushes the non-wetting phase back through the invading wetting phase and overcomes the capillary pressure generated by interfaces at the open face. This process, referred to as counter-current imbibition, is one mechanism by which oil is displaced from the rock in fractured reservoirs (Morrow & Mason, 2001). The mass balance requirement for counter-current imbibition means that the net volumetric flows of the two fluids are equal but in opposite directions.

Counter-current imbibition in reservoir rocks is usually studied at the core level using cylindrical cores about 75mm in length and about 37mm in diameter. In fundamental studies of displacement mechanisms, the initial condition is often of complete saturation with oil. In tests of more practical interest, cores usually contain a low initial water saturation with the remaining pore space filled with oil. The core is immersed in brine and the volume of expelled oil is measured. Results are recorded as cumulative oil production versus time. In practice, experiments are easier to conduct if the core has all faces of the cylinder open to the invading phase. However, even under the ideal condition of a homogeneous porous media, this gives complex flow patterns which are awkward to model. In order to compare experimental results for the effect of changing interfacial tension (σ), fluid viscosities (μ_w and μ_{nw}), sample shape, rock porosity (φ), permeability (K) and the size, shape and boundary conditions, various scaling groups have been proposed. Ma *et al* (1997) incorporated most of these factors into a dimensionless time t_D as in Eq. 8.1.

$$t_{\mathrm{D}} = \frac{1}{L_{\mathrm{c}}^2}\sqrt{\frac{K}{\varphi}}\frac{\sigma}{\sqrt{\mu_{\mathrm{w}}\mu_{\mathrm{nw}}}}t \qquad 8.1$$

Size, shape, and boundary conditions are included as the characteristic length L_c:

$$L_c = \sqrt{\frac{V_{\text{total}}}{\sum_{i-1}^{i=n} \frac{A_i}{x_i}}} \qquad 8.2$$

where V_{total} is the total volume, A_i is the area open to imbibition in the *i*th direction, x_i is the distance travelled by the imbibition front from the open surface to the no-flow boundary and *n* is the total number of surfaces open to imbibition. The correlation appears to work quite well (Yildiz et al., 2006). For a cylinder open on all faces this equation gives (Zhang et al. 1996)

$$L_c = \frac{L_{\text{core}} d}{2\sqrt{d^2 + 2L_{\text{core}}^2}} \qquad 8.3$$

where L_{core} is the core length and *d* is the core diameter. The correlation simply brings the production data on a $\log_{10} t$ scale together by moving the curves left and right. It does not change their shape and so does not allow cores of different geometry to have different shaped production-time curves.

The standard analysis of the flow of two phases through a porous material requires three functions: capillary pressure and the relative permeabilities, to the wetting and non-wetting phases. All are solely functions of saturation. In addition, for perfect counter-current imbibition, the flow of one phase is exactly equalled by the reverse flow of the other phase.

Direct observation indicates that one-dimensional counter-current imbibition, particularly for cores with no initial water saturation, can be primarily a frontal process (Li et al., 2006) and so, as a limiting case, we could imagine that ALL of the saturation change takes place at the saturation front where there is a step change in saturation from S_{wi} (the initial wetting phase saturation) to S_{wf} (the wetting phase saturation behind the front). The assumption makes imbibition piston-like and means that, behind the front, the relative permeabilities of each of the two phases are constant. Also, behind the front at one instant in time, the flow of wetting phase (q_w) is invariant with distance from the open face and consequently the flow of non-wetting phase (q_{nw}) is similarly invariant but in the opposite direction. Darcy's law gives the two flows:

$$q_{\text{w}} = -\frac{K k_{\text{rw}} A}{\mu_{\text{w}}} \frac{\partial P_{\text{w}}}{\partial x} \qquad 8.4$$

$$q_{\text{nw}} = -\frac{K k_{\text{rnw}} A}{\mu_{\text{nw}}} \frac{\partial P_{\text{nw}}}{\partial x} \qquad 8.5$$

where *K* is the permeability, k_{rw} and k_{mw} are the relative permeabilities to the respective phases, μ_w and μ_{nw} are the respective viscosities, *A* is the area and *x* is a distance. The

capillary pressure P_c is the difference between the pressure in the non-wetting phase (P_{nw}) and the pressure in the wetting phase (P_w).

$$P_{\mathrm{c}} = P_{\mathrm{nw}} - P_{\mathrm{w}} \tag{8.6}$$

Perfect counter-current flow implies:

$$q_{\mathrm{w}} = -q_{\mathrm{nw}} \tag{8.7}$$

Combining Eq.(8.4) to Eq.(8.7) gives:

$$q_{\mathrm{w}} = \frac{K k_{\mathrm{rw}} k_{\mathrm{rnw}} A}{\mu_{\mathrm{w}} k_{\mathrm{rnw}} + \mu_{\mathrm{nw}} k_{\mathrm{rw}}} \frac{\partial P_{\mathrm{c}}}{\partial x} \tag{8.8}$$

Because behind the front the saturation has been assumed to be constant, q_w will not vary between the open face and the front. Let M be a mobility factor and let

$$M = \frac{k_{\mathrm{rw}} k_{\mathrm{rnw}}}{\mu_{\mathrm{w}} k_{\mathrm{rnw}} + \mu_{\mathrm{nw}} k_{\mathrm{rw}}} \tag{8.9}$$

For constant saturation, the factor M will be constant and so Eq. 8.8 can be integrated between the open face and the front to give

$$q_{\mathrm{w}} \int_0^{x_{\mathrm{f}}} \frac{\mathrm{d}\, x}{A} = KM\left(P_{\mathrm{cf}} - P_{\mathrm{co}}\right) \tag{8.10}$$

Where P_{cf} is the effective capillary pressure at the imbibition front, and P_{co} is the effective capillary pressure at the open face. At the open face the pressure in the wetting phase is zero but the pressure in the non-wetting phase is not zero because the non-wetting phase forms bubbles as it exits the rock.

For cylindrical tubes, the capillary pressure is related to permeability by the Leverett (1941) relation:

$$P_{\mathrm{c}} = \sigma \sqrt{\frac{\varphi}{2K}} \tag{8.11}$$

Eq. 8.10 contains a difference in capillary pressures, P_{cf} - P_{co}. The capillary pressure at the front, $P_{cf,}$ is mainly produced by the smaller pores and the capillary pressure at the open face, $P_{co,}$ is mainly produced by the larger pores. The difference between them is thus related to the spread of the pore size distribution of the rock. For a spread of pore sizes, P_{cf} - P_{co} , can be related to the mean capillary pressure, P_c, by a factor C_{spread} which is in some way determined by the breadth and shape of the pore size distribution. For narrow pore size distributions, C_{spread} will be small and for wide pore size distributions C_{spread} will be large. We thus obtain

$$P_{\mathrm{cf}} - P_{\mathrm{co}} = C_{\mathrm{spread}} \sigma \sqrt{\frac{\varphi}{2K}} \tag{8.12}$$

Eliminating P_{cf} - P_{co} from Eq.1.10 gives

$$q_{\mathrm{w}} \int_0^{x_{\mathrm{f}}} \frac{\mathrm{d}\,x}{A} = KMC_{\mathrm{spread}}\sigma\sqrt{\frac{\varphi}{2K}} \qquad 8.13$$

The flow of wetting phase arriving at the front advances the position of the front and the local mass balance gives:

$$\frac{\mathrm{d}x_{\mathrm{f}}}{\mathrm{d}t} = \frac{q_{\mathrm{w}}}{\varphi A_{\mathrm{f}}\left(S_{\mathrm{wf}} - S_{\mathrm{wi}}\right)} \qquad 8.14$$

Where x_f is the distance of the front from the open face and A_f is the area of the front.

Eliminating q_w between Eq. 8.13 and Eq.8.14 gives

$$\int_0^{x_{\mathrm{f}}} \left(\int_0^{x_{\mathrm{f}}} \frac{\mathrm{d}\,x}{A} \right) A_{\mathrm{f}}\,\mathrm{d}\,x_{\mathrm{f}} = \sqrt{\frac{K}{2\varphi}}\,\frac{MC_{\mathrm{spread}}\sigma}{\left(S_{\mathrm{wf}} - S_{\mathrm{wi}}\right)}t \qquad 8.15$$

This is the fundamental equation used in the subsequent analysis.

Practical situations

Linear imbibition

For linear imbibition into a cylindrical core open at one end, the cross-sectional area is everywhere constant, making A equal A_f. Hence integration of Eq. 8.15.gives

$$x_{\mathrm{f}}^2 = \sqrt{\frac{2K}{\varphi}}\,\frac{MC_{\mathrm{spread}}\sigma}{\left(S_{\mathrm{wf}} - S_{\mathrm{wi}}\right)}t \qquad 8.16$$

showing that the distance that the front advances is proportional to $\sqrt{time}$, a well-known result for the situation in the absence of gravity before a dispersed front has reached the end of a core (Washburn, 1921; Reis & Cil, 1993; Li et al., 2003; Tavassoli et al., 2005). The time, t_{end}, taken for the front to reach the end of the core at distance L_{max} is

$$t_{\mathrm{end}} = L_{\mathrm{max}}^2\sqrt{\frac{\varphi}{2K}}\,\frac{\left(S_{\mathrm{wf}} - S_{\mathrm{wi}}\right)}{MC_{\mathrm{spread}}\sigma} \qquad 8.17$$

Eq. 8.17 gives the characteristic length for linear imbibition as L_{max}, which agrees exactly with the characteristic length predicted by Eq. 8.2.

Radial imbibition

For radial flow into a cylinder with capped ends, the area A will vary with the distance that the front has penetrated and so the function for the amount of imbibition *vs* time will be different from linear imbibition. Let the core length be L_{core} and its radius R_{max}, and let the front penetrate to a distance x_f at time t. At distance x into the core the area is. Eq. 8.15 can $2\pi\left(R_{\mathrm{max}} - x\right)L_{\mathrm{core}}$ be integrated to give

$$R_{\max}^2 + 2R_{\mathrm{f}}^2 \ln\frac{R_{\mathrm{f}}}{R_{\max}} - R_{\mathrm{f}}^2 = 2\sqrt{\frac{2K}{\varphi}}\frac{MC_{\mathrm{spread}}\sigma}{\left(S_{\mathrm{wf}} - S_{\mathrm{wi}}\right)}t \qquad 8.18$$

From geometry, the fraction of the total imbibition when the front is at R_f is

$$f = 1 - \left(\frac{R_{\mathrm{f}}}{R_{\max}}\right)^2 \qquad 8.19$$

The time taken for the front to reach the centre of the core (the no-flow boundary) when imbibitions stops, t_{end}, is

$$t_{\mathrm{end}} = \frac{R_{\max}^2}{2}\sqrt{\frac{\phi}{2K}}\frac{\left(S_{\mathrm{wf}} - S_{\mathrm{wi}}\right)}{MC_{\mathrm{spread}}\sigma} \qquad 2.5$$

For radial imbibition the characteristic length is thus $R_{\max}/\sqrt{2}$ and this also agrees exactly with the characteristic length predicted by Eq. 8.2.

Spherical imbibition

For radial imbibition into a spherical core, radius R_{sphere}, the area at distance x into the core is and $4\pi\left(R_{\max} - x\right)^2$ integration of Eq. 8.15 gives:

$$R_{\mathrm{sphere}}^2 - 3R_{\mathrm{f}}^2 + 2\frac{R_{\mathrm{f}}^3}{R_{\mathrm{sphere}}} = 3\sqrt{\frac{2K}{\varphi}}\frac{MC_{\mathrm{spread}}\sigma}{\left(S_{\mathrm{wf}} - S_{\mathrm{wi}}\right)}t \qquad 8.20$$

when the front R_f is at (i.e. R_{max} - x) at time t. The fraction f of total imbibition when the front is at R_f is

$$f = 1 - \left(\frac{R_{\mathrm{f}}}{R_{\mathrm{sphere}}}\right)^3 \qquad 8.21$$

The time for the front to reach the centre of the sphere is

$$t_{\mathrm{end}} = \frac{R_{\mathrm{sphere}}^2}{3}\sqrt{\frac{\phi}{2K}}\frac{\left(S_{\mathrm{wf}} - S_{\mathrm{wi}}\right)}{MC_{\mathrm{spread}}\sigma} \qquad 8.22$$

For imbibition into a sphere the characteristic length is $R_{sphere}/\sqrt{3}$ and this agrees exactly with the characteristic length predicted by Eq. 8.2. It is also the same as predicted by Eq. 8.3 when the core has the same diameter as its length. Thus compared to a cylinder sealed on all faces but one end, a sphere fills three times faster, provided the maximum distance the front has to travel is the same.

The functional forms of the production *vs* time functions for linear, radial and spherical imbibition are quite different but, on the conventional log_{10} *time* scale, they are only slightly different (see Fig. 8.1). They can be compared in several ways. The first (Fig. 8.1) is without the adjustment for characteristic length.

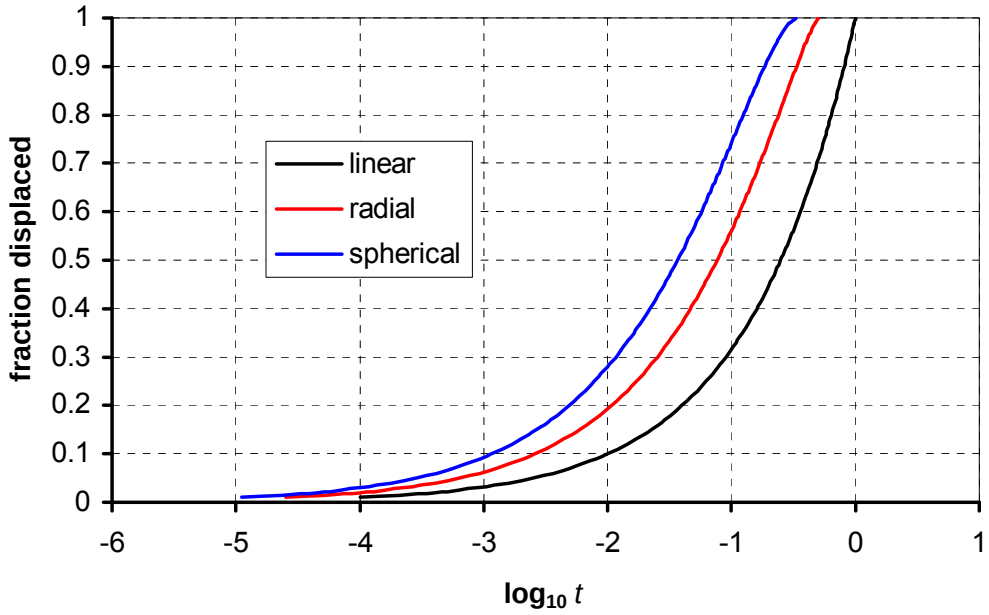

Figure 8.1. The fraction imbibed versus $\log_{10} t$ for linear, radial and spherical imbibition. The factor $\sqrt{\frac{2K}{\varphi}}\frac{MC_{\text{spread}}\sigma}{(S_{\text{wf}}-S_{\text{wi}})}$ has been set at 1. No adjustment for the different characteristic lengths has been made. The core length (for one end open) and radius (for radial and spherical) are also unity so that the distance the front has to travel is the same for all geometries. The sequence of shapes is similar to that given by Zimmerman et al. (1990).

If the characteristic length is incorporated, then the shape differences of the imbibition curves are more apparent (Fig. 8.2).

The $\log_{10}$ time axis is useful because a constant factor only moves the curve left or right. It does not change its shape. However, the differences between the curves are better shown on a $\sqrt{t}$ plot on which the linear imbibition becomes a straight line (Fig. 8.3).

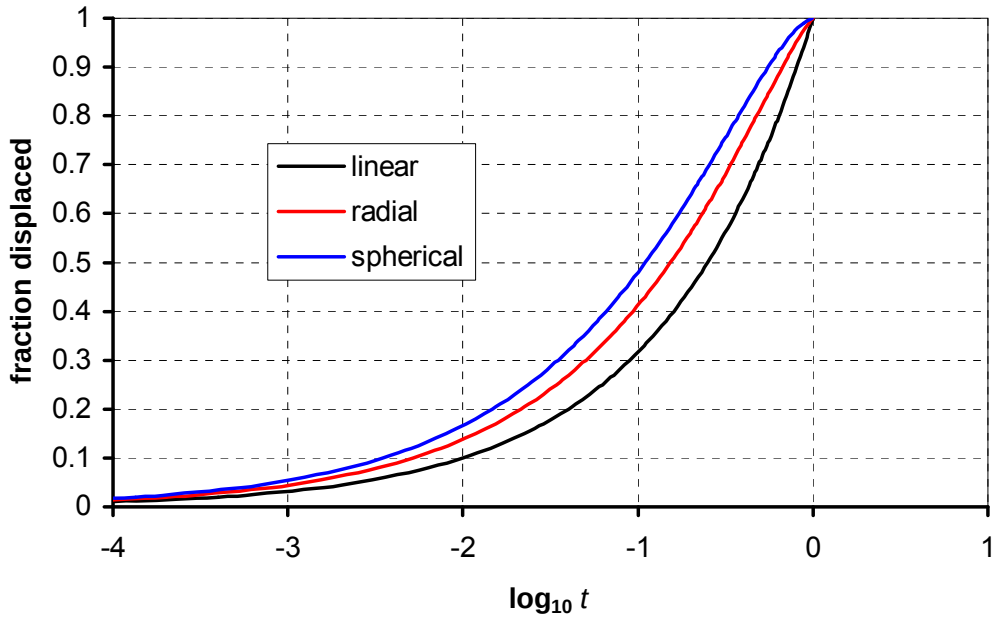

Figure 8.2 Imbibition curves after the characteristic length factor has been incorporated. This makes the time at which imbibition is complete the same and illustrates the similarity in shape between all of the curves. As expected the sphere imbibes fastest on average but slows most at the end.

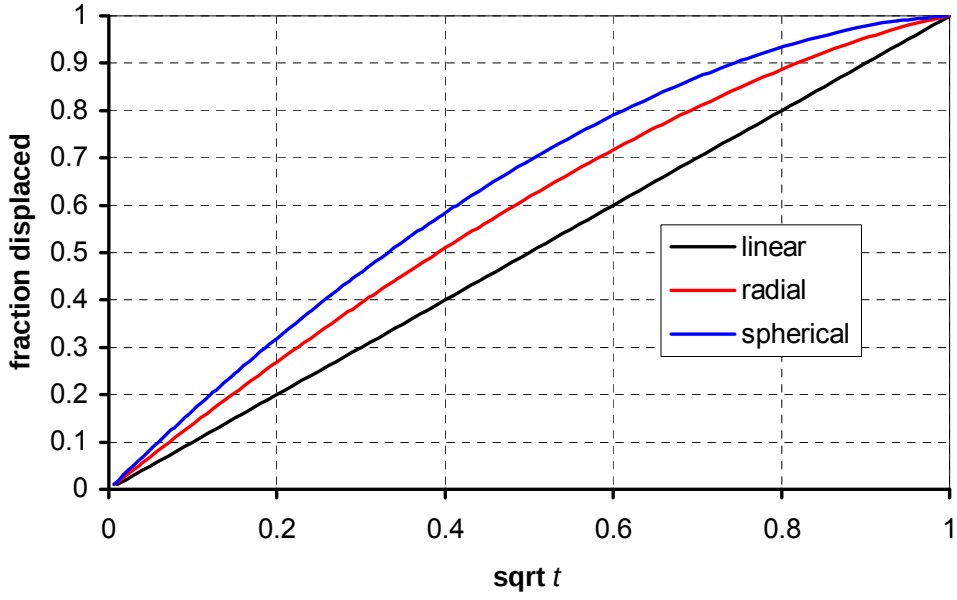

Figure 8.3. The imbibition curves of Fig. 2 plotted against $\sqrt{t}$. This plot enhances the differences in shape.

Conical imbibition

Frontal imbibition into a cylindrical core with all faces open can be modelled by considering the likely position of the no-flow boundary with respect to linear flow from each end and radial imbibition from the cylindrical surface. For each end, imbibition can be modelled by flow into a cone with the front advancing from the open end with the tapering conical face sealed. From the cylindrical outer face there will be radial imbibition into the remains of the cylinder (termed a toroid ring). If the core is long enough then the conical region swept by imbibition will be a full cone. However, if the half length of the core is less than the core radius then the conical imbibition region will reach the center plane of the core (and its mirror image at the other end) before the full cone is developed. This means that the imbibition from the cylindical surface will not reach the axis of the core before the core axis is enveloped by imbibition from the ends. The imbibition fronts define two cases; a long toroid ring with complete cones, and a short toroid ring that contains truncated cones (see Fig. 8.4).

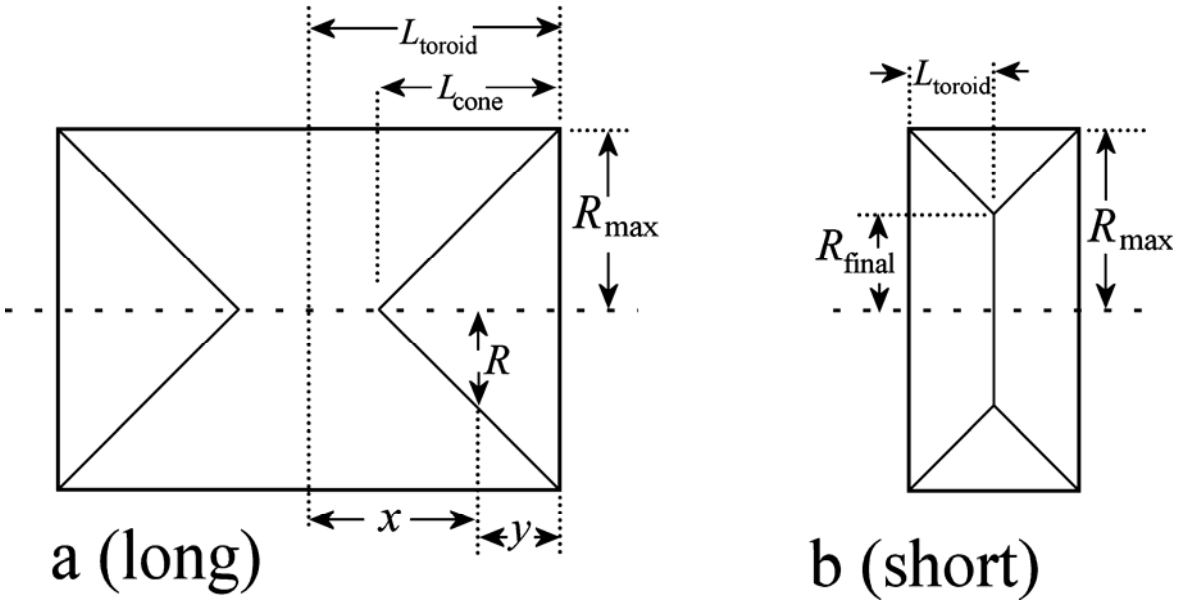

Figure 8.4. Diagram showing a section through a long (a) and short (b) core. The core is considered to have two imbibition regimes. The first is linear into a cone at each end, and the second is radial into the residual outer toroid. For a long core, the cones are completely filled just as the radial flow reaches the center axis. For the short core they are truncated because the fronts in each cone meet before the radial imbibition front reaches the core axis. The angle of the cone is determined by the requirement that the time taken for complete imbibition in the two regimes is the same.

The complete cone has an open base, radius, R_{max}, and the conical face is sealed. Its length is L_{cone}. At some distance y in from the base (see Fig. 4a), a section through the cone is a circle of radius R and area πR^2. Integration of Eq. 1.15 with y in place of x gives

$$\left(\frac{L_f}{L_{cone}}\right)^2 - \frac{2}{3}\left(\frac{L_f}{L_{cone}}\right)^3 = \frac{1}{L_{cone}^2}\sqrt{\frac{2K}{\varphi}}\frac{MC_{spread}\sigma}{(S_{wf} - S_{wi})}t \qquad 8.22$$

when the position of the front is at a distance L_f from the open face at time t. The fraction f of total imbibition when the front is at L_f is the ratio of the volume of the cone truncated at a length L_f divided by the volume of the complete cone:

$$f = 1 - \left(1 - \frac{L_\mathrm{f}}{L_\mathrm{cone}}\right)^3 \qquad 8.23$$

The time for the front to reach the end of the cone is

$$t_\mathrm{end} = \frac{L_\mathrm{cone}^2}{3}\sqrt{\frac{\phi}{2K}}\frac{\left(S_\mathrm{wf} - S_\mathrm{wi}\right)}{MC_\mathrm{spread}\sigma} \qquad 8.24$$

Numerically therefore, imbibition into a cone is very similar to imbibition into a sphere. The characteristic length for a cone is $L_\mathrm{cone}/\sqrt{3}$ which also agrees with the prediction of Eq. 8.2. Interestingly, and usefully because it simplifies later equations, it is independent of the angle of the cone.

Imbibition into a long toroid

For one half-length of the cylindrical core, the toroid ring is the space around the outside of the complete cone. The toroid has its outer cylindrical face open and the conical face sealed. The remaining circular face at half-length is also sealed, making this like one half of an all-faces-open core. Let the toroid have a length L_{toroid} (which is half of the cylinder length) and a radius R_{max}.

From the curved outer face of the cylinder there is radial imbibition into a space of decreasing area (because the boundary of the cone is sealed). From Fig. 8.4a the distance from the half-length of the core to a point on the cone at radius R is given by:

$$x = L_\mathrm{toroid} - L_\mathrm{cone} + \frac{L_\mathrm{cone}}{R_\mathrm{max}}R \qquad 8.25$$

To simplify let $a = L_\mathrm{toroid} - L_\mathrm{cone}$ and $b = L_\mathrm{cone}/R_\mathrm{max}$. The analysis follows the same pattern as before. For the toroid ring, at some general radius, R, the area, A_R, through which the flow q_w^R is passing is the area of the cylinder of length x

$$A_\mathrm{R} = 2\pi Rx = 2\pi R(a + bR) \qquad 8.26$$

Integration of Eq. 8.15 using this expression gives

$$\left[\left[\frac{1}{2}R_{\mathrm{f}}^2+\frac{1}{3}\frac{bR_{\mathrm{f}}^3}{a}\right]\ln\left[\frac{(a+bR_{\max})}{(a+bR_{\mathrm{f}})}\frac{R_{\mathrm{f}}}{R_{\max}}\right]+\frac{1}{6}\left(\frac{a}{b}\right)^2\left[\ln(a+bR_{\mathrm{f}})-\frac{bR_{\mathrm{f}}}{a}-\left(\frac{bR_{\mathrm{f}}}{a}\right)^2\right]\right]_{R_{\max}}^{R_{\mathrm{f}}}$$
$$=\frac{1}{2}\sqrt{\frac{2K}{\varphi}}\frac{MC_{\mathrm{spread}}}{(S_{\mathrm{wf}}-S_{\mathrm{wi}})}t_{\mathrm{f}} \qquad 8.27$$

The time, t_f, is when the front has reached R_f. The time when the axis is reached, t_{end} is:

$$t_{\mathrm{end}}=\frac{R_{\max}^2}{3}\left(\left(\frac{L_{\mathrm{toroid}}}{L_{\mathrm{cone}}}-1\right)^2\ln\left(1-\frac{L_{\mathrm{cone}}}{L_{\mathrm{toroid}}}\right)+\frac{L_{\mathrm{toroid}}}{L_{\mathrm{cone}}}\right)\sqrt{\frac{\varphi}{2K}}\frac{(S_{\mathrm{wf}}-S_{\mathrm{wi}})}{MC_{\mathrm{spread}}\sigma} \qquad 8.28$$

The characteristic length is thus $\frac{R_{\max}}{\sqrt{3}}\sqrt{\left(\frac{L_{\mathrm{toroid}}}{L_{\mathrm{cone}}}-1\right)^2\ln\left(1-\frac{L_{\mathrm{cone}}}{L_{\mathrm{toroid}}}\right)+\frac{L_{\mathrm{toroid}}}{L_{\mathrm{cone}}}}$. This expression differs from the characteristic length given by Eq. 8.2.

Imbibition into a short toroid

If the half-length of the core is less than the radius, then the imbibition front coming into the cones from the opposite ends of the core meet before the radial imbibition reaches the core axis (Fig. 8.4b). Thus, when the radial imbibition does not reach the core axis, the region of imbibition from the ends correspond to a truncated cone. The radius where the cone is truncated at the mid-point of the cylinder is R_{final}. The analysis is similar to the long toroid but the integrals have different limits. The basic equation for imbibition into the toroid Eq. 8.14 is unchanged and gives

$$\left[\left[\frac{1}{2}R_{\mathrm{f}}^2+\frac{1}{3}\frac{bR_{\mathrm{f}}^3}{a}\right]\ln\left[\frac{(a+bR_{\max})}{(a+bR_{\mathrm{f}})}\frac{R_{\mathrm{f}}}{R_{\max}}\right]+\frac{1}{6}\left[\left(\frac{a}{b}\right)^2\ln(a+bR_{\mathrm{f}})-\frac{a}{b}R_{\mathrm{f}}-R_{\mathrm{f}}{}^2\right]\right]_{R_{\max}}^{R_{\mathrm{final}}}=$$
$$\frac{1}{2}\sqrt{\frac{2K}{\varphi}}\frac{MC_{\mathrm{spread}}\sigma}{(S_{\mathrm{wf}}-S_{\mathrm{wi}})}t_{\mathrm{end}} \qquad 8.29$$

Evaluation gives

$$t_{\mathrm{end}}=\left(\frac{1}{3}R_{\mathrm{final}}^2\ln\frac{R_{\mathrm{final}}}{R_{\max}}+\frac{1}{3}R_{\max}^2\left(1-\frac{R_{\mathrm{final}}}{R_{\max}}\right)\right)\sqrt{\frac{\varphi}{2K}}\frac{(S_{\mathrm{wf}}-S_{\mathrm{wi}})}{MC_{\mathrm{spread}}\sigma} \qquad 8.30$$

Thus, for the short toroid ring, the characteristic length is $\frac{R_{\mathrm{final}}}{\sqrt{3}}\sqrt{\ln\frac{R_{\mathrm{final}}}{R_{\max}}+\frac{R_{\max}^2}{R_{\mathrm{final}}^2}-\frac{R_{\max}}{R_{\mathrm{final}}}}$, which is not the same as the prediction of Eq. 8.2.

Cylindrical imbibition

Imbibition into a core with all faces open can be broken down into two parts. From the flat ends there is a conical imbibition region. From the outer cylindrical surface there is imbibition into the remaining toroid. Imbibition into the cylinder is the sum of imbibition into the external surface of the toroid and into the end of the cone. For a long core, it will take the same time, t_{end}, for the front in the cone to reach the cone apex as it takes for the front in the toroid ring to reach the core axis. For the short core, the times are the same when the front is at R_{final}.

For the long core, t_{end} for the cone given by Eq. 8.11 will be the same as t_{end} for the toroid given by Eq. 8.28. Equating these two imbibition times gives

$$t_{\text{end}} = \frac{R_{\max}^2}{3}\left(\left(\frac{L_{\text{toroid}}}{L_{\text{cone}}}-1\right)^2 \ln\left(1-\frac{L_{\text{cone}}}{L_{\text{toroid}}}\right)+\frac{L_{\text{toroid}}}{L_{\text{cone}}}\right)=\frac{L_{\text{cone}}^2}{3} \qquad 8.31$$

By elimination of t_{end} the resulting equation gives the length of the conical section as a function of the length of the cylinder and its radius. Unfortunately Eq. 8.31 is only explicit for $L_{\text{cone}}/R_{\max}$. However, for a given value of $L_{\text{cone}}/L_{\text{toroid}}$, we can calculate $R_{\max}/L_{\text{cone}}$ using Eq. 8.31 and, since we know $L_{\text{cone}}/L_{\text{toroid}}$, we can find the aspect ratio of the core $L_{\text{toroid}}/R_{\max}$. Now, knowing R_{max}, the left hand side of Eq. 8.27 can be evaluated and t_f can be found for any given value of R_f using

$$\left[\frac{1}{2}R_{\text{f}}^2+\frac{1}{3}\frac{bR_{\text{f}}^3}{a}\right]\ln\left[\frac{(a+bR_{\max})}{(a+bR_{\text{f}})}\frac{R_{\text{f}}}{R_{\max}}\right]+\frac{1}{6}\left[\left(\frac{a}{b}\right)^2\ln\left(\frac{a+bR_{\text{f}}}{a+bR_{\max}}\right)-\frac{a}{b}(R_{\text{f}}-R_{\max})-(R_{\text{f}}^2-R_{\max}^2)\right]$$
$$=\frac{1}{2}\sqrt{\frac{2K}{\varphi}}\frac{MC_{\text{spread}}\sigma}{(S_{\text{wf}}-S_{\text{wi}})}t_{\text{f}} \qquad 8.32$$

At this value of t_f, the front will have advanced a distance L_f into the cone. The time for this is given by Eq. 8.23 and is given by

$$L_{\text{cone}}^2\left(\left(\frac{L_{\text{f}}}{L_{\text{cone}}}\right)^2-\frac{2}{3}\left(\frac{L_{\text{f}}}{L_{\text{cone}}}\right)^3\right)=\sqrt{\frac{2K}{\varphi}}\frac{MC_{\text{spread}}\sigma}{(S_{\text{wf}}-S_{\text{wi}})}t_{\text{f}} \qquad 8.33$$

Since t_f and L_{cone} are known, Eq. 8.33, a cubic, can be solved to find L_f. All of the dimensions are then known and the fraction of the cylinder invaded by the displacing phase can be found from the sum of the volume imbibed by the toroid and the volume imbibed by the cone

$$f=1-\left(\frac{R_{\text{f}}}{R_{\max}}\right)^2\left(1-\frac{L_{\text{cone}}}{L_{\text{toroid}}}\right)-\frac{L_{\text{cone}}}{L_{\text{toroid}}}\left(\frac{2}{3}\left(\frac{R_{\text{f}}}{R_{\max}}\right)^3+\frac{1}{3}\left(1-\left(\frac{L_{\text{f}}}{L_{\text{cone}}}\right)^3\right)\right) \qquad 8.34$$

For the short core the situation is slightly different. As before, the time for the front to reach R_{final}, its final position at the half-length of the core, will be the same as the time for the front from the flat end to reach the mid-point of the core (L_{toroid}). From Eq. 8.23 for the cone, this time is

$$t_{\text{end}} = L_{\text{cone}}^2 \left[\left(\frac{L_{\text{toroid}}}{L_{\text{cone}}} \right)^2 - \frac{2}{3} \left(\frac{L_{\text{toroid}}}{L_{\text{cone}}} \right)^3 \right] \sqrt{\frac{\varphi}{2K}} \frac{\left(S_{\text{wf}} - S_{\text{wi}} \right)}{MC_{\text{spread}}\sigma} \qquad 8.35$$

And changing the limits in Eq. 8.27, for the toroid

$$\left[\left[\frac{1}{2} R_{\text{f}}^2 + \frac{1}{3} \frac{bR_{\text{f}}^3}{a} \right] \ln \left[\frac{\left(a + bR_{\text{max}} \right)}{\left(a + bR_{\text{f}} \right)} \frac{R_{\text{f}}}{R_{\text{max}}} \right] + \frac{1}{6} \left[\left(\frac{a}{b} \right)^2 \ln\left(a + bR_{\text{f}} \right) - \frac{a}{b} R_{\text{f}} - {R_{\text{f}}}^2 \right] \right]_{R_{\text{max}}}^{R_{\text{final}}}$$

$$= \frac{1}{2} \sqrt{\frac{2K}{\varphi}} \frac{MC_{\text{spread}}\sigma}{\left(S_{\text{wf}} - S_{\text{wi}} \right)} t_{\text{end}} \qquad 8.36$$

Evaluation gives

$$t_{\text{end}} = \left(\frac{1}{3} R_{\text{final}}^2 \ln \frac{R_{\text{final}}}{R_{\text{max}}} + \frac{1}{3} R_{\text{max}}^2 \left(1 - \frac{R_{\text{final}}}{R_{\text{max}}} \right) \right) \sqrt{\frac{\varphi}{2K}} \frac{\left(S_{\text{wf}} - S_{\text{wi}} \right)}{MC_{\text{spread}}\sigma} \qquad 8.37$$

The characteristic length is thus $\frac{R_{\text{final}}}{\sqrt{3}} \sqrt{\ln \frac{R_{\text{final}}}{R_{\text{max}}} + \frac{R_{\text{max}}^2}{R_{\text{final}}^2} - \frac{R_{\text{max}}}{R_{\text{final}}}}$. If the two values of t_{end} from Eq. 8.35 and Eq. 8.37 are equal, they can be eliminated. Also, simple geometry gives

$$\frac{L_{\text{toroid}}}{L_{\text{cone}}} = 1 - \frac{R_{\text{final}}}{R_{\text{max}}} \qquad 8.38$$

and so

$$t_{\text{end}} = \frac{1}{3} R_{\text{final}}^2 \ln \frac{R_{\text{final}}}{R_{\text{max}}} + \frac{1}{3} R_{\text{max}}^2 \left(1 - \frac{R_{\text{final}}}{R_{\text{max}}} \right) = L_{\text{toroid}}^2 \left(1 - \frac{2}{3} \left(1 - \frac{R_{\text{final}}}{R_{\text{max}}} \right) \right) \qquad 8.39$$

If we make R_{max} = 1 and take a value for R_{final} (less than 1) then Eq. 8.39 is explicit for L_{toroid}. We now know the core aspect ratio, L_{toroid} /R_{max}. Once L_{toroid} is known, the length of the apex of the cone can be found using Eq. 8.38. For any intermediate value of front position R_f, we can now use Eq. 8.32 to find the appropriate t_f and the cubic Eq. 8.33 to find L_f. As before, the fraction of the core filled with invading phase can be found from Eq. 8.34

Comparison of the predictions for all-faces-open

For the special case of a cylindrical core of length equal to its diameter, the equations given above simplify to give behaviour similar to that of a sphere (Eq. 8.29). However, if the core

is longer or shorter than its diameter then behaviour tends to that of a core with one end open when it is short, and to that of a core with both ends closed as the length of the cylinder increases.

Shape of the production curve
Figure 8.5 shows production curves for imbibition into cylindrical cores with all-faces-open for a range of aspect ratios. The shapes of the curves are all very similar. Experiments show much the same behaviour.

Figure 8.6 shows these examples plotted as the square root of time divided by the characteristic length given by Eq. 8.28 and Eq. 8.30. As expected these functions are all similar and show the core with the lowest aspect ratio tending towards linear imbibition.

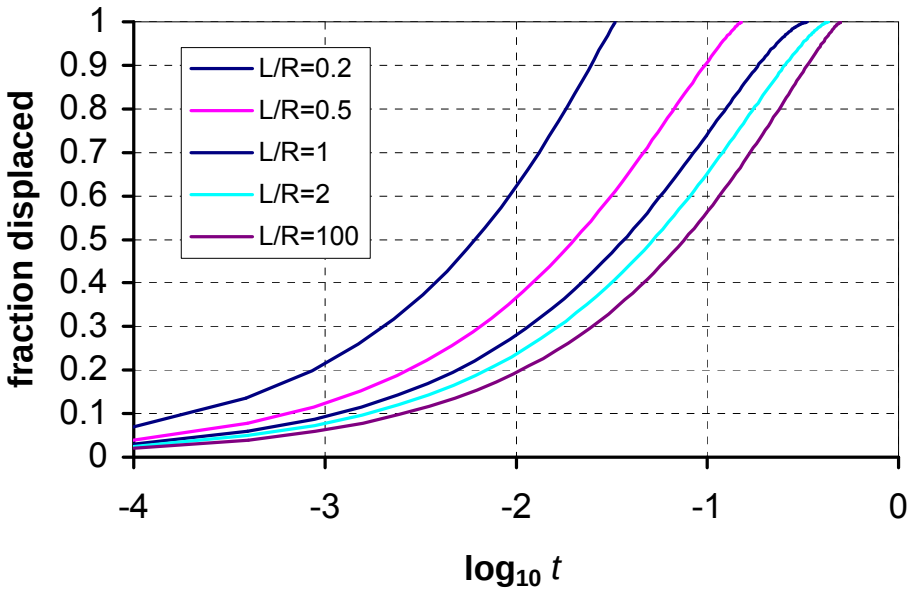

Fig 8.5. Examples of imbibition into all-faces-open cores with unit radius. Again, the factor $\sqrt{\frac{2K}{\varphi}\frac{MC_{\text{spread}}\sigma}{(S_{\text{wf}}-S_{\text{wi}})}}$ **has been set at 1. When *L*/*R* is large, imbibition is essentially radial; when *L*/*R* is unity there is spherical imbibition and when *L*/*R* is small, imbibition is linear. *L* is the half-length of the core.**

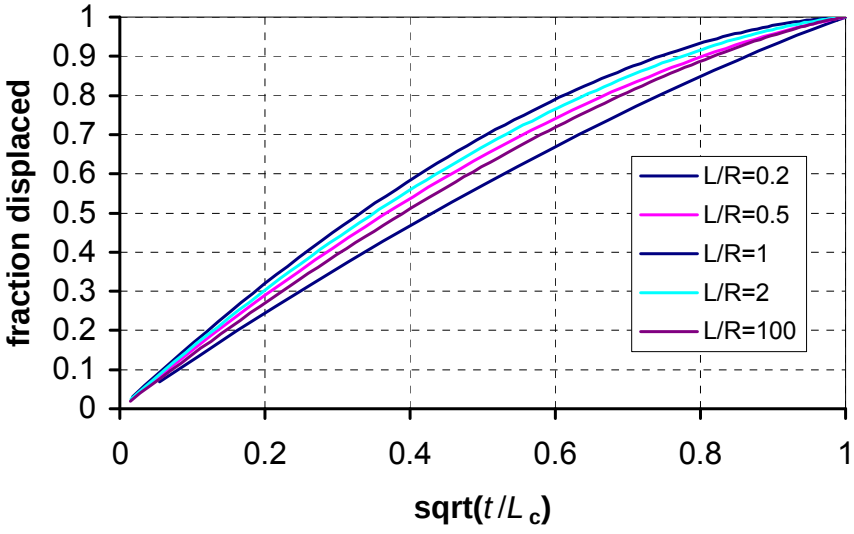

Figure 8.6. Examples of all-faces-open imbibition plotted using the square root of time and scaling using the characteristic length. For an aspect ratio of 0.2 (*L*/*R*=0.2), imbibition tends towards the linear case, for *L*/*R*=100, the radial case and for *L*/*R*=1, the spherical case. A core with all faces open and with a *L*/*R* ratio of 0.35 has almost exactly the same normalised production curve as a core with two ends closed (radial imbibition).

Comparison of the characteristic lengths

Eq. 8.3 gives Ma's characteristic length for an all-faces-open core as

$$L_c = \frac{L_{core} d}{2\sqrt{d^2 + 2L_{core}^2}} \qquad 8.3$$

For a core with a diameter greater than its length, the characteristic length given by the combination of a cone and toroid ring is

$$L_c = \frac{R_{final}}{\sqrt{3}} \sqrt{\ln \frac{R_{final}}{R_{max}} + \frac{R_{max}^2}{R_{final}^2} - \frac{R_{max}}{R_{final}}} = L_{toroid} \sqrt{1 - \frac{2}{3}\left(1 - \frac{R_{final}}{R_{max}}\right)} \qquad 8.40$$

with

$$\frac{L_{toroid}}{L_{cone}} = 1 - \frac{R_{final}}{R_{max}} \qquad 8.37$$

For a core with a diameter less than its length

$$L_c = \frac{R_{max}}{\sqrt{3}} \sqrt{\left(\frac{L_{toroid}}{L_{cone}} - 1\right)^2 \ln\left(1 - \frac{L_{cone}}{L_{toroid}}\right) + \frac{L_{toroid}}{L_{cone}}} = \frac{L_{cone}}{\sqrt{3}} \qquad 8.40$$

The characteristic lengths from these functions are compared on Fig. 8.7. They show close agreement. The percentage difference between the characteristic length given by the Ma

relationship and the cone/toroid model is shown on Fig. 8.8. The difference is less than 7% and only 2% for cores with a typical aspect ratio of about 2. However, imbibition times depend on the square of the characteristic length, and so in experiments, the differences in time would be approximately doubled. Even so, it is unlikely that the differences would be detectable in standard experiments. Figure 8.9 gives the correction factor by which the characteristic length calculated from the Ma equation should be multiplied to make it agree with the cone/toroid model.

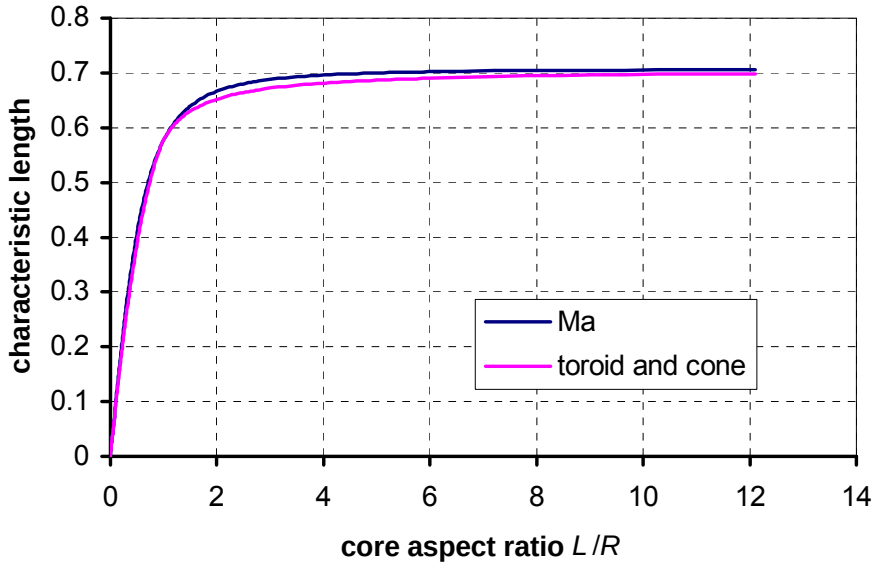

Figure 8.7. Comparison of the characteristic length predicted by Ma's equation (Eq.(8.3)) with that from the current toroid and cone analysis. The two are very similar. The Ma characteristic length is always greater than, or equal to, the characteristic length of the cone/toroid model.

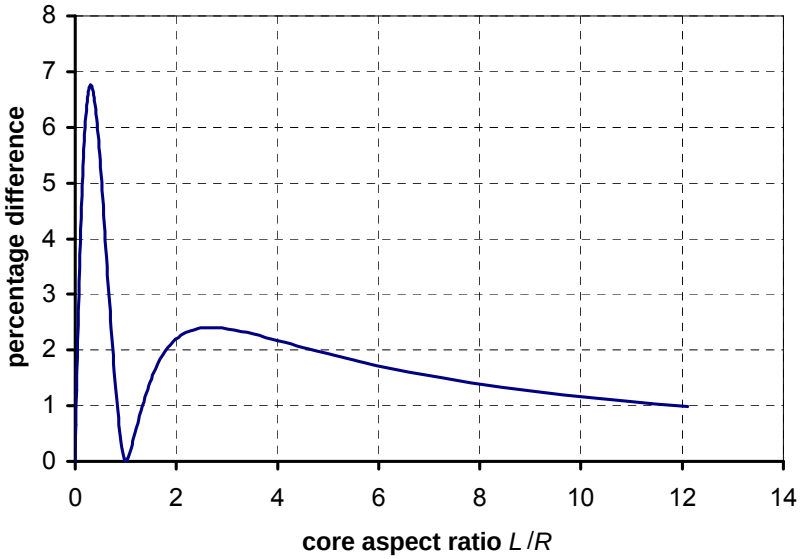

Figure 8.8. The percentage increase (see Fig. 8.7) in the Ma characteristic length required for agreement with the toroid/cone analysis.

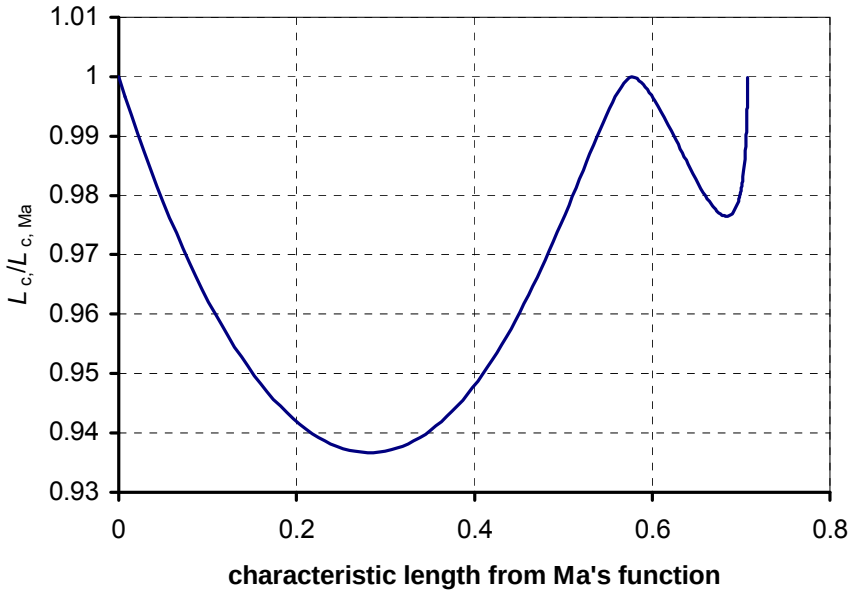

Figure 8.9. The correction factor by which the characteristic length calculated from the Ma equation has to be multiplied to bring it into agreement with the cone/toroid model.

Comparison with experiments

It is clear that there are only subtle differences in shape between production curves from cores with different boundary conditions and so only repeated averaged experiments might show the differences. One such set of experiments has been reported by Fischer and Morrow (2005). The experiments were on cores of the same sandstone with almost identical size and shape. The only parameter that was intentionally varied was the viscosity of the two fluids, one being mineral oil and the other a brine. The viscosity of the brine was made to match the viscosity of the oil by the addition of glycerol. This made dramatic variation of the viscosity (4-170cp) possible with only relatively small changes to interfacial tension. It was found that the results scaled quite well, as expected (Ruth et al. (2004)), by the dimensionless time given in Eq. 8.1. However, for our purposes the results are sufficient in number and correlate so well that they do show the small changes in the shapes of the production curves predicted by the core/toroid model. Figure 8.10 shows the results taken from Fischer and Morrow (2005) for the all-faces open cores. The aspect ratio (L/R) was about 1.7 in all cases.

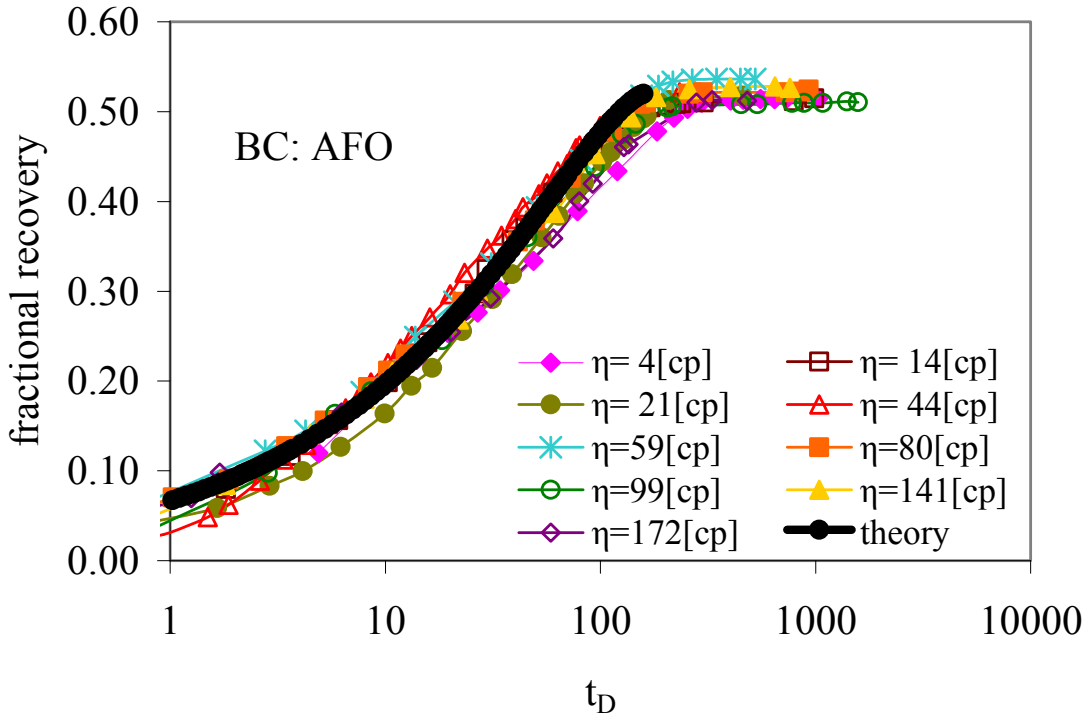

Figure 8.10. The experimental data of Fisher and Morrow (2005) for cores with all faces open, matched viscosities, and an aspect ratio of 1.7, are shown compared to the predictions of the cone/toroid theory. The theory assumes piston-like displacement and includes a single properties factor optimised to give the best fit to this data.

Because there is an unknown constant linking the dimensionless time with the cone/toroid theory, the theory line can be moved left and right on the $\log_{10}$ graph to find the position which gives the best fit to the experimental data. In Fig. 8.10 the fit is generally as good as the data, and falls within the range of the data points. The same comparison is made for cores with two ends closed (giving radial imbibition) in Fig. 8.11. Again the theory does not go outside the spread of the data, although the data is slightly more spread than for the all-faces-open cores. The same properties constant as in Fig. 8.10 has been used. Finally, the results for one-end-open geometry (giving linear imbibition) are shown in Fig. 8.12, again using the same properties constant as in Fig. 8.10. The fit is not quite as good but this is only in regard to the position of the theory line; its shape is almost perfect.

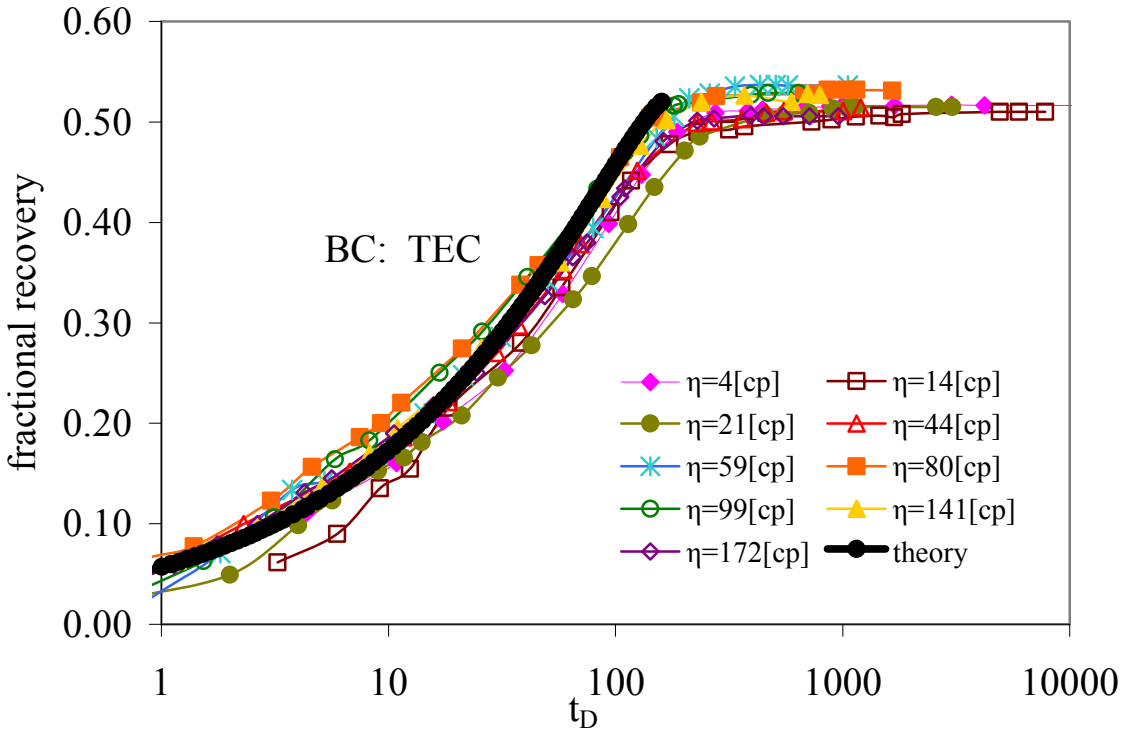

Figure 8.11. The experimental data of Fisher and Morrow (2005) for cores with matched viscosities and the boundary condition of two ends closed. The same constant has been used to place the theory curve as in Fig 8.10.

So why does the assumption of piston-like displacement work so well? One reason is that analytically, for linear imbibition, there is a self-similar front for much of the displacement and the distance advanced by any fixed saturation is proportional to the square root of time (Tavassoli et al., 2005; Ruth et al., 2007). It is only when the leading edge of the front reaches the end of the core that a saturation versus $\sqrt{time}$ plot will deviate from a straight line. For radial imbibition the front is not exactly self-similar (Standnes, 2006) but is a close approximation to it. Furthermore, the volume involved as the front approaches the centre is proportionally quite small, with the last 25% of the distance corresponding to only 6% of the volume. The second reason is that, in most experiments, there is no initial water saturation and a significant fraction of the brine reaching the front is used to raise the brine permeability from zero, thus giving a front sharpening effect.

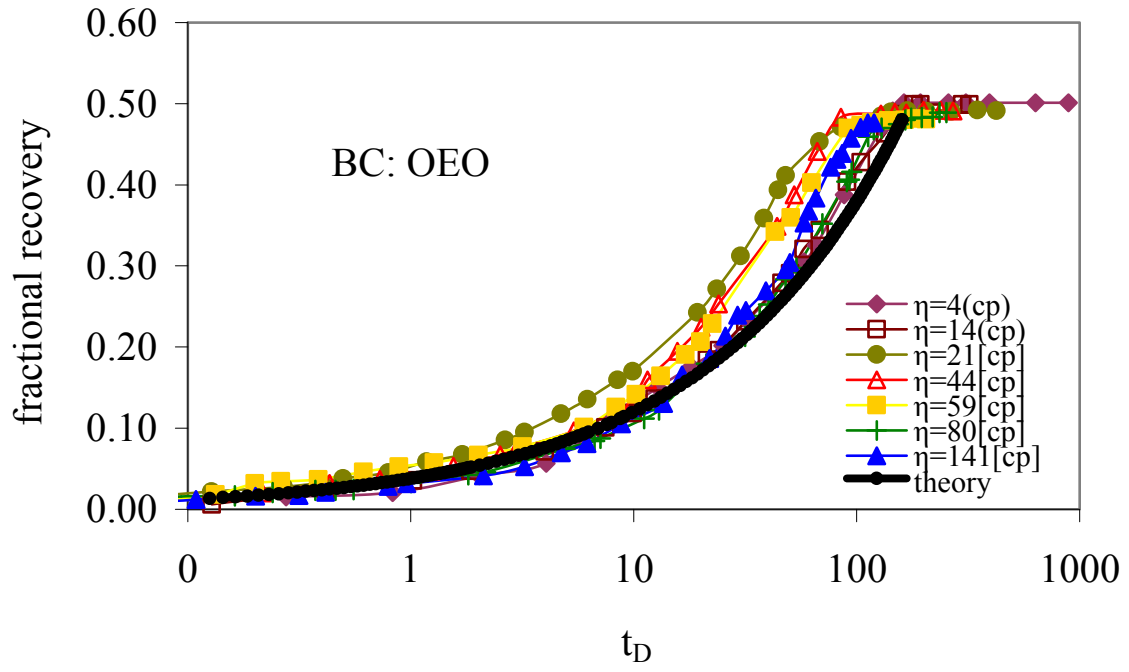

Figure 8.12. The experimental data of Fisher and Morrow (2005) for cores with matched viscosities and the boundary condition of one end open. The same constant has been used to place the theory curve as in Figs 8.10 and 8.11. In this case it places the curve slightly too far to the right. The shape, however, is almost perfect. When plotted against the square root of dimensionless time, all of the experimental points give straight lines except at late times.

REFERENCES

Fischer, H. and Morrow, N.R., 2005. "Scaling of oil recovery by spontaneous imbibition for matched viscosities" SPE96812, SPE Annual Technical Conference, Dallas, TX, Oct. 9-12, 2005.

Leverett, M.C., 1941. Capillary behavior in porous solids, Trans Am. Inst. Min. & Met. Eng. **142**, 152-169

Li, Y., Morrow, N.R., Ruth, D., 2003. Similarity solution for linear counter-current spontaneous imbibition. J. Pet. Sci. Eng. **39**, 309-326.

Li, Y, Ruth, D., Mason, G., Morrow, N.R., 2006. Pressures acting in counter-current spontaneous imbibition. J. Pet. Sci. Eng, **52**, 87-99.

Ma, S., Morrow, N.R., Zhang, X., 1997. Generalized scaling of spontaneous imbibition data for strongly water-wet systems. J. Pet. Sci. Eng. **18**, 165-178.

Morrow, N.R. & Mason, G., 2001. Recovery of oil by spontaneous imbibition, Current Opinion in Colloid & Interface Science **6**, 321-337.

Reis, J.C. & Cil, M., 1993. A model for oil expulsion by counter-current water imbibition in rocks: one-dimensional geometry. J. Pet. Sci. Eng., **10**, 97-107.

Ruth, D.W., Mason, G., Morrow, N, Li, Y., 2004. The effect of fluid viscosities on counter-current spontaneous imbibition, Proceedings of the Society of Core Analysts Symposium, Abu Dhabi, SCA2004-11. 1-13. http://www.scaweb.org/assets/papers/2004_papers/SCA2004-11.pdf

Ruth, D.W., Yu, L., Mason, G. & Morrow, N.R., 2007. An approximate analytical solution for counter-current spontaneous imbibition. Transp. Porous Media **66**, 373-390.
Standnes, D.C., 2006. Spontaneous imbibition of water into cylindrical cores with high aspect ratio: Numerical and experimental studies. J. Pet. Sci. Eng. **50**, 151-160.
Tavassoli, Z, Zimmerman, R.W., & Blunt, M.J., 2005. Analytic analysis for oil recovery during counter-current imbibition in strongly water-wet syatems. Transp. Porous Media **58**, 173-189
Yildiz, H.O., Gokmen, M, & Cesur, Y., 2006. Effect of shape factor, characteristic length, and boundary conditions on spontaneous imbibition. J. Pet. Sci. Eng. **53**, 158-170.
Zhang, X., Morrow, N.R., Ma, S., 1996. Experimental verification of a modified scaling group for spontaneous imbibition, SPERE, **11**, 280-285.
Zimmerman, R.W., Bodvarsson, G.S., 1990. Absorption of water into porous blocks of various shapes and sizes. Water Resources Research, **26**, 2797-2806.

Task 9. *Increased oil recovery by spontaneous imbibition.*

Background

The effect of boundary conditions has been investigated with respect to the capillary pressure that resists oil production at the rock face. The capillary back pressure was reduced by lowering the oil/water interfacial tension by means of low concentration surfactant. The capillary backpressure will be lowered in proportion to the interfacial tension lowering. The effect of reduced back-pressure on rate of recovery has been measured. This is one of three examples of how improved fundamental understanding can lead to new approaches to improved oil recovery from fractured reservoirs.

Experiments

Initial studies have been performed on Berea sandstone, a relatively homogeneous rock for which imbibition under very strongly water wet conditions is well characterized. Core properties are listed in Table 9.1. The oil was purified Soltrol 220 mineral oil (an isoparaffin oil) with polar components removed by flow through silica gel. A 10,000 *ppm* NaCl brine (viscosity of 0.00102 *Pa.s*) was used to ensure compatibility with the chosen surfactant. Tomadol 9-18 Alcohol Ethoxylate is a commonly used nonionic surfactant, which gives large but not extreme lowering of interfacial tension.

The imbibition tests were run on cores with one end face open. Addition of surfactant caused oil to be produced as an emulsion. During the surfactant imbibition stages of the tests, shaking or other means of removing produced oil from the core end face were never attempted. The collected sample was heated at $80^{o}C$ to break the emulsion before determining the volume of produced oil.

Interfacial tensions

The brine/Soltrol 220 interfacial tension was 47 *mN*/*m*. Interfacial tensions measured after addition of surfactant for concentrations of 0, 30, 100, 375, 750, 1500, and 3000 are plotted in

Fig. 9.1. A concentration of the 3,000 *ppm*, giving an interfacial tension of 2.19 *mN*/*M,* was adopted for the first series of experiments on core plugs. This concentration is well above the CMC (Fig. 9.1).

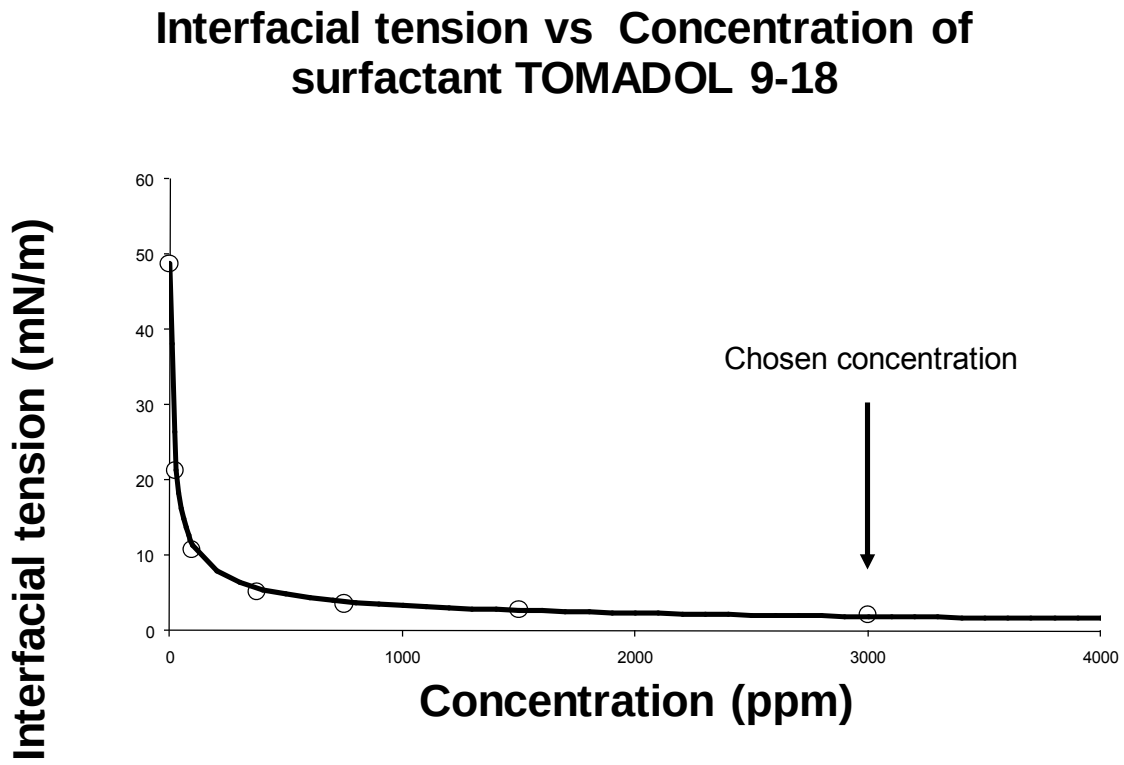

Fig. 9.1 Interfacial tension vs concentration for surfactant TOMADOL 9-18

Brine/oil COUCSI

A Berea sandstone core plug (NS1) of 3.755 cm diameter and about 6.51 cm length, with porosity of 17% and permeability of 0.073 μm^2 was tested (see Table 1). The core was initially saturated with Soltrol 220. The interfacial tension between oil and brine was 48.8 *mN/m*.

Core: NS1

The core was initially saturated with refined oil and then immersed in brine. COUCSI caused the end pressure, $P_{end,}$ to rise quickly to 6.5 *kPa* within 1.5 *hours*. After P_{end} had reached 7 *kPa* it remained constant until the front reached the end of the core 15.8 *hours* after immersion. The oil recovery of Q_o/V_ϕ was 0.362 OOIP when the imbibition front reached the end of the core (Fig. 9.2). The rate of oil recovery then showed marked decay and the end pressure (P_{end}) decreased. P_{end} eventually dropped to 0.3 *kPa* about 96 *hours* after the start of imbibition. The final oil recovery Q_o/V_ϕ was 0.435 OOIP.

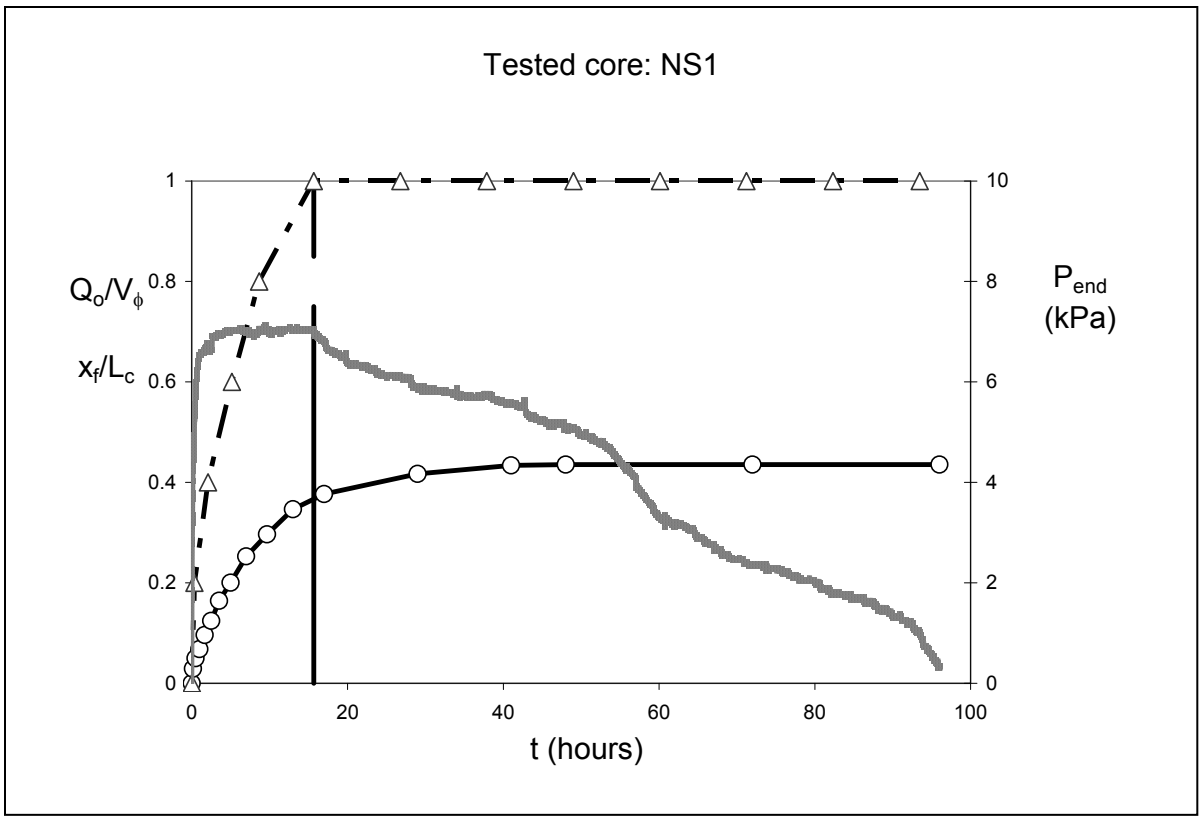

Fig. 9.2 Distance of advance of the imbibition front, oil recovery and end pressure versus time for recovery of refined oil by spontaneous imbibition.

Initial refined oil/brine COUCSI followed by immersion in surfactant solution

Core: IS1

Stage I: Refined oil/brine COUCSI

First the open end Core IS1 was immersed in brine. As for test NS1, P_{end} quickly rose to 6.6 *kPa* in the first 2 *hours*. When the front had advanced 2.67 cm from the open face (0.4 x_f/L_c), the oil recovery Q_o/V_ϕ was 0.168 OOIP (Fig. 9.3). The results up to this stage were similar to those for test NS1.

Stage II: Imbibition of surfactant solution

Frontal flow period in surfactant brine

Upon immersion of Core IS1in surfactant solution, the rate of imbibition increased and the end pressure (P_{end}) dropped from 6.6 *kPa* to 4 *kPa.* . The produced oil soon changed from large to very small drops. The oil was collected in an inverted funnel in the form of an emulsion. Even with the initial period of brine invasion, the front arrived at the end of the core, 5.1 *hours* after immersion in surfactant solution. This was almost three times faster than required (13.6 hours) for the front to reach the end of the core in Test NS1 (see Fig. 9.2). At this time the oil recovery, Q_o/V_ϕ, was 0.362 OOIP. The volume of oil produced was determined by reducing the volume of produced emulsion by the ratio of the volume of demulsified oil to the volume of emulsion determined at the end of the test.

Stage III: Imbibition of surfactant after frontal flow
After the front arrived at the end of the core, the end pressure (P_{end}) continued to drop and after 3 *hours* had decreased down to its lowest value of 3.7 *kPa*. Then the end pressure (P_{end}) rose again to a peak value of 5.48 *kPa* over the next 3.1 *hours*. Over the next 32 *hours*, the end pressure (P_{end}) gradually dropped to 0.25 *kPa*. The final oil recovery was 0.472 OOIP. In addition to faster recovery, the recovery was 3.7% OOIP higher than that for core NS1. Immersion in surfactant even after establishing initial frontal flow of surfactant free brine caused increase oil recovery.

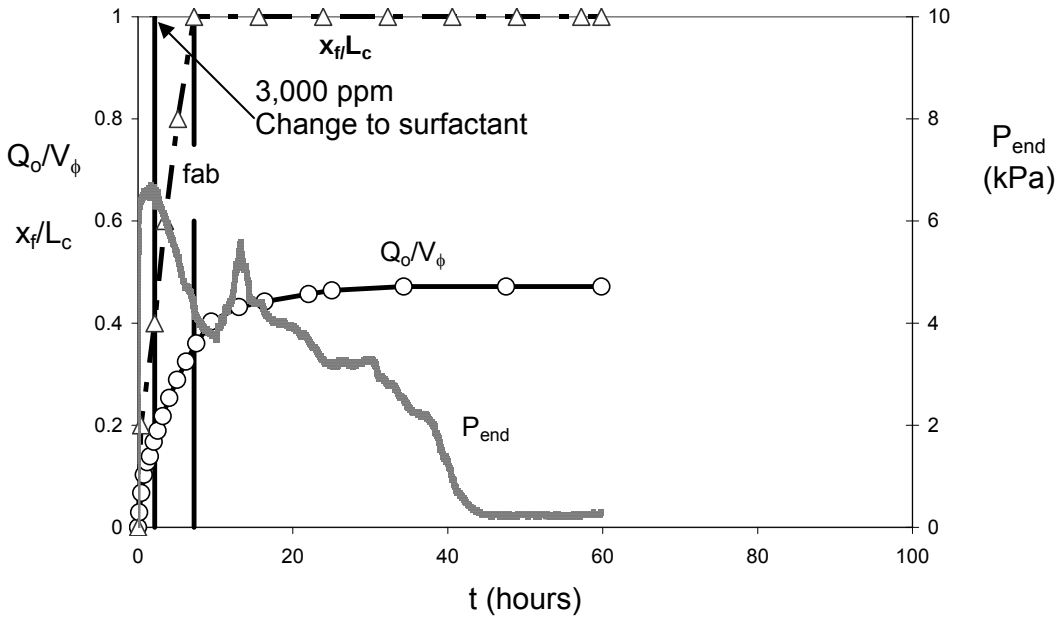

Fig. 9.3 COUCSI with initial invasion of brine followed by surfactant solution (core IS1).

Core: IS2
The test for Core IS2 was a duplicate of that for core IS1.

Stage I: Refined oil/brine COUCSI
After immersion of the OEO core in brine, the front reached advanced 2.67 cm from the open face ($x_f/L_c = 0.4$) after 2 *hours*. By this time the end pressure, P_{end} had risen to 6.7 *kPa* and 15.2% OOIP had been produced (Fig. 9.4).

Stage II: Imbibition of surfactant
After immersion in surfactant solution, the front advanced from 0.4 of the core length to the end of the core in 6.35 *hours*. P_{end} fell from 6.7 to about 4.1 *kPa* within three hours and remained close to this value until the front reached the end of the core. The additional oil recovery during that period was 0.363 OOIP.

Stage III: Imbibition of surfactant after frontal flow
At the end of frontal flow, the pressure drop increased sharply from 4.2 *kPa* to a peak value of 5.22 *kPa* in the next 2 *hours* and decreased to a second minimum of 2.32 *kPa* in the next *13.5 hours.* After that, P_{end} then increased to the second peak value of 3 *kPa* over the next 11 *hours* and decreased to 0.3 *kPa* after the next 13.2 *hours*. Finally P_{end} increased to a third peak value of 0.8 *kPa* in the next 11 *hours* and decreased to a stable value of 0.23 *kPa* after the next 5 *hours*. After correction for the volume of oil contained in the produced emulsion, the final oil recovery was 0.47 OOIP.

Test IS2 gave 3.9% OOIP additional oil recovery compared to the non-surfactant COUCSI in core NS1. It seems that the enhanced recovery was produced by imbibition of surfactant solution subsequent too the frontal flow period. Considering the complexity of the tests, reproducibility of results for the duplicated tests is reasonable.

After completion of COUCSI, 2 cc of brine were produced from the dead end of the core. The interfacial tension was 17.1 *mN/m*. From the interfacial tension versus concentration behavior (Fig. 9.1), this indicated that concentration in the aqueous phase had been reduced 50 fold, from 3000 *ppm* at the core inlet to about 60 *ppm* at the outlet.

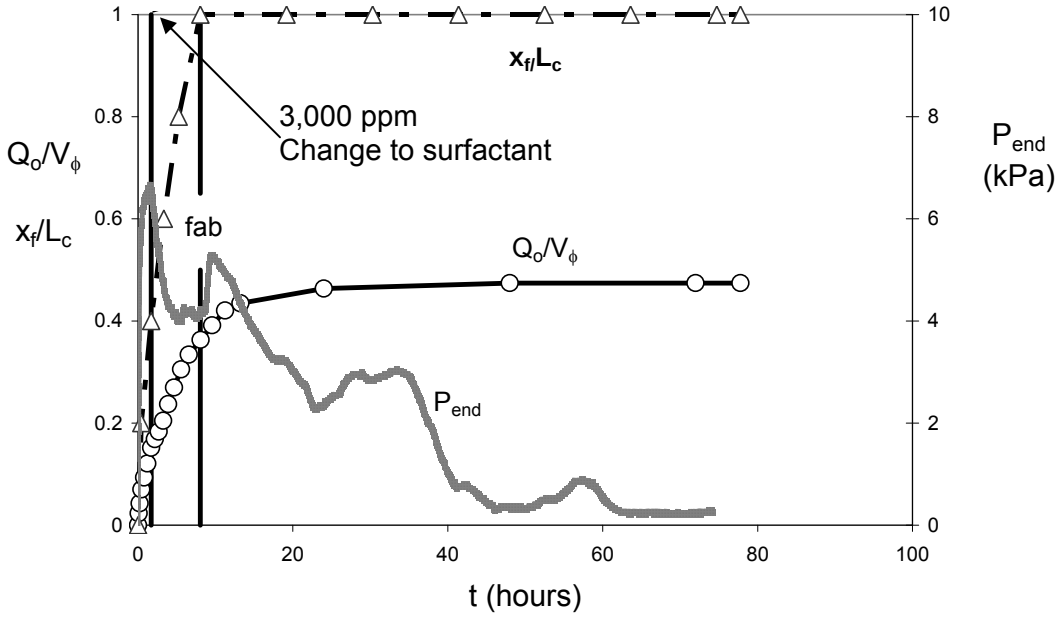

Fig. 9.4 COUCSI with initial invasion of brine followed by surfactant (core IS2).

III. Imbibition of surfactant solution
Imbibition of surfactant COUCSI was tested for two Berea sandstones cores (see Table 9.1) that were initially saturated with refined oil.

Core: DS1

Stage I: Frontal flow
An oil-saturated core was immersed directly in surfactant solution. Oil was produced as very small droplets that were collected as an emulsion. Even though surfactants reduce the interfacial tension, the recovery rate was slightly faster than the rate for non-surfactant COUCSI (Test NS1) before the front reached the end of core (14.8 *hrs* as compared to15.7 *hours* in Test NS1). P_{end} quickly rose to 1.25 *kPa* in the first 1.5 *minutes* and held close to constant at about 1.4 *kPa* and then rose slightly to 1.5 *kPa* just before the front reached the end of the core. The end pressure (P_{end}) during frontal flow was five times lower than that for Test NS1. When the imbibition front reached the end of the core the oil recovery had reached 0.365 OOIP (Fig. 9.4).

Stage II: Post contact period in surfactant brine
After the frontal flow period, the end pressure (P_{end}) increased to reach a maximum of 4.97 *kPa* after 8 *hours* and remained close to this value for a further 8 *hrs*. Then P_{end} gradually dropped to 1.48 *kPa* over the next 87.5 *hours*.

The final oil recovery was 0.508 OOIP. Surfactant imbibition resulted in 7.1% OOIP additional oil recovery compared to recovery by imbibition of brine (Test NS1).

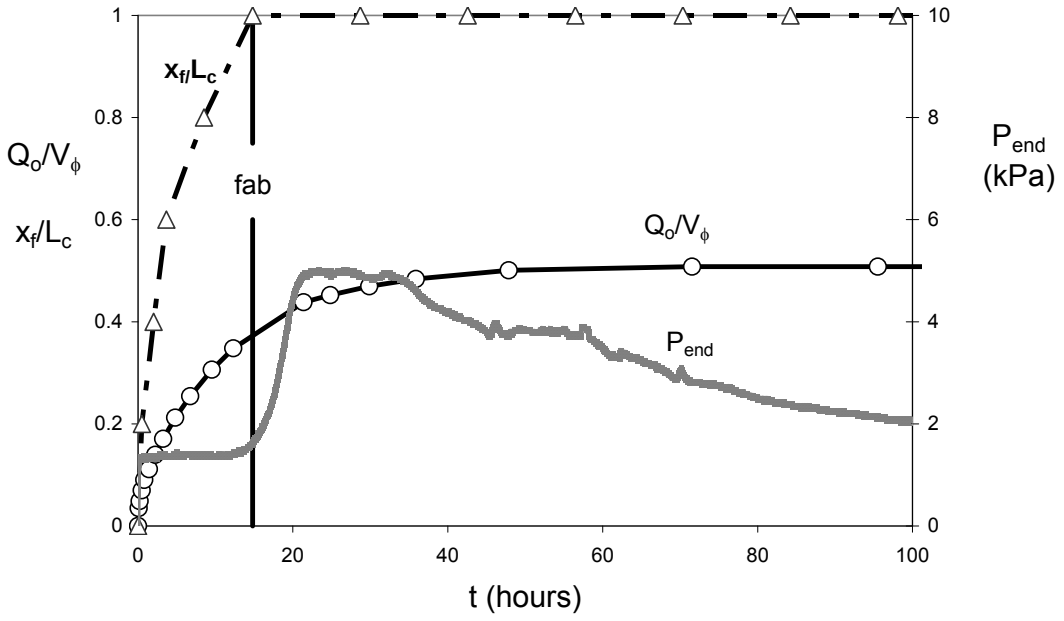

Fig. 9.5 Imbibition of surfactant by COUCSI for initially-oil-saturated core DS1.

Core: DS2
The test for Core DS2 was a duplicate of that for DS1.

Stage I: Frontal flow
Except for slightly faster flow, the recovery and end pressure response was similar to that for Test DS1 during frontal flow. The front arrived at the end of the core after 13 *hours*. The oil recovery reached 0.361 OOIP during the frontal flow period (Fig. 9.5). The produced oil was in the form of an emulsion that was somewhat more translucent than for Test DS1. P_{end} remained at about 1.55 *kPa* until the front had almost reached the end of the core.

Stage II: Post contact recovery
The end pressure rose slowly for 5 *hours* after completion of frontal flow and then rapidly, to a maximum of 4.81 *kPa* in the next 7.9 *hours*. Then P_{end} gradually dropped to about 1.7 *kPa* after 45 *hours* and then more slowly with minor fluctuation to 0.9 *kPa* over the next 25 *hours*. The final oil recovery was 0.481 OOIP. Recovery was 5% OOIP higher than for imbibition of brine (Core NS1).

The interfacial tension of the effluent brine against oil after completion of COUCSI was 14.25 *mN/m*.

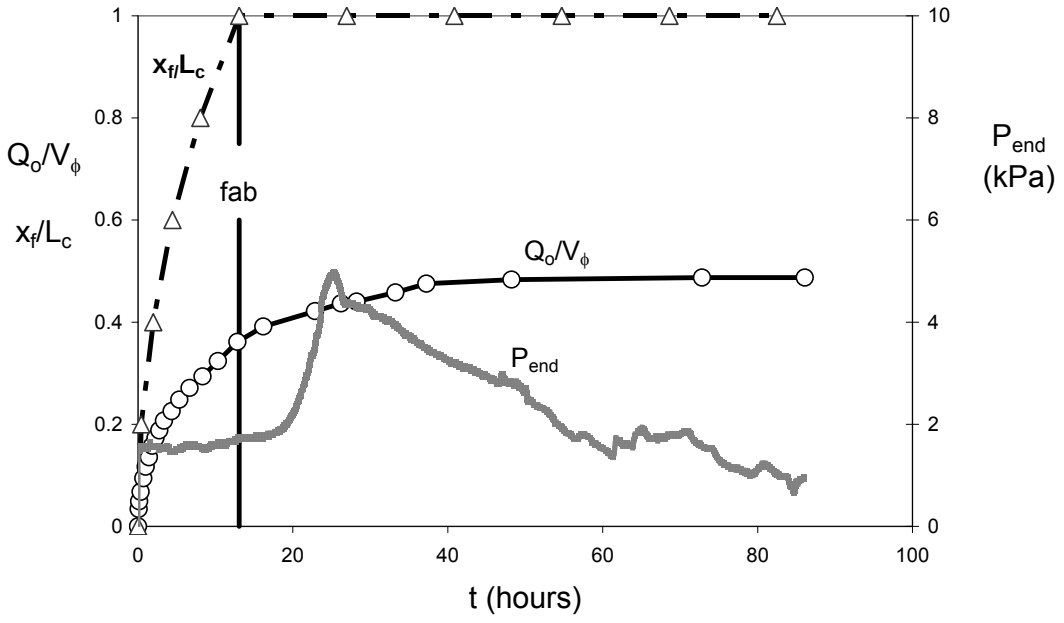

Fig. 9.6 Imbibition of surfactant by COUCSI for initially-oil-saturated core DS1.

Table 9.1. Core properties, oil recovery, and end pressure

EXPERIMENT	CORE	d (cm)	L_c (cm)	ϕ (%)	K (μm^2)	R at fab	R after fab	Pend at fab (kPa)	Max Pend after fab (kPa)
Aqueous phase	NS1	**3.755**	**6.51**	**17.3**	**0.072**	**0.362**	**0.435**	**7.0**	**7.0**
Brine/Surfactant Solution	IS1	**3.788**	**6.674**	**17.2**	**0.071**	**0.362**	**0.472**	**4.3**	**5.4**
	IS2	**3.781**	**6.686**	**17.2**	**0.070**	**0.363**	**0.474**	**4.3**	**5.2**
Surfactant Solution	DS1	**3.786**	**6.531**	**17.2**	**0.070**	**0.365**	**0.508**	**1.7**	**5.0**
	DS2	**3.785**	**6.521**	**17.2**	**0.071**	**0.361**	**0.483**	**1.7**	**4.9**

CONCLUSIONS

Task 6

1. Monitoring the end pressure for one-end-open linear imbibition under conditions of restricted COUCSI provides an estimate of the capillary pressure acting at the imbibition front under dynamic conditions.
2. After limited invasion of WP, the end pressure in the NWP remains essentially constant as the WP redistributes by simultaneous imbibition and drainage without change in the overall brine content.
3. The capillary pressures at the oil/water displacement front ranged from 6.6 to 21.3 *kPa* for Berea sandstones with permeabilities between 1.067 and 0.06 μm^2. Frontal capillary pressures for different Berea sandstones did not give a straight forward correlation with permeability as would be given by rocks of similar pore geometry.

Task 7

4. A new design of imbibition cells has been built and tested.

Task 8

5. Analytical solutions were developed with the assumption that displacement by imbibition can be modeled as a piston-like front with provision for flow of the non-wetting phase. Cylindrical cores, the most commonly tested sample shape were modeled as two cones and a residual torroidal ring. Shape factors calculated with the model are close to the semi-empirical values proposed by Ma et al. (1977). Theoretical predications give a reasonable fit to experimental data.
6. Production versus time curves can be predicted with the model.

Task 9

7. Novel results of the change in imbibition end pressure for surfactant solutions are presented.
8. Even though interfacial tensions are reduced, the rate and amount of oil recovery by imbibition of surfactant solution are increased.
9. Changes in end pressures that accompany imbibition of surfactant solutions provide quantitative information on surfactant adsorption from the rise in interfacial tension.